TSPE16010-006-12

지난 1000 년간 남극진동의 변동성에 대한 연구

Variations of Antarctic Oscillation during the past millennium and the twenty first century

아칸소스대학교

제 출 문

극지연구소장 귀하

본 보고서를 “과거, 현재의 극지기후 관측과 재현을 통한 기후변화 메커니즘 규명 연구”과제의 위탁연구“지난 1000 년간 남극진동의 변동성에 대한 연구”과제의 최종보고서로 제출합니다.

2016. 12.

총괄연구책임자 : 김성중

위탁연구기관명 : 아칸소스대학교

위탁연구책임자 : 송 펭 (song Feng)

위탁참여연구원 : 장용준 (Zhang Yongjun)

Changes in winter severity in the Southern Hemisphere during the 20th and 21st centuries

Abstract

Winter seasons have significant societal impacts across all sectors ranging from direct human health to ecosystems, transportation, and recreation. This study quantifies the severity of winter and its spatial-temporal variations in the Southern Hemisphere (SH) using the newly developed Accumulated Winter Season Severity Index (AWSSI). This index, based on daily weather data, accounts the impacts of cold temperature and snowfall/snow depth to quantify the severity of winter. Our results suggested that the snowfall and snow depth can be reasonably estimated using daily temperature and precipitation when both quantities are missing. The estimated snowfall and snow depth can be subsequently used to determine the AWSSI. The temperature dominant the AWSSI variations in the southern hemisphere. During the last century, the winter in the southern Africa, Australia, New Zealand and coastal Antarctic become less severe. Harsher winters are identified in majority of the Antarctica, while the trend in winter conditions in the southern South America (SSA) show mixed results. The EOF analysis suggested that the winter severity in SSA is closely linked to ENSO and the temperature changes in the SH.

The simulations the 21 CMIP5 models can well capture the spatial and temporal variations of the observed changes in winter severity during 1951-2005. The models are consistently in projecting a future milder winter under the RCP4.5 and 8.5 scenarios. The AWSSI is projected to decrease 30-50% in SSA, 50-60% in the southern Africa, 40-50% in Australia and New Zealand, and 10-20% in Antarctica by the end of this century under

RCP4.5 scenario. The projected decrease in winter severity is more pronounced under the RCP8.5 scenario.

Motivation and goals

The severity as well as the start and end of winter can greatly affect the energy use, transportation and public health (Changnon, 1979; Mansikkaniemi, 1979; Andrey et al., 2003; Rauber et al., 2013; Huang and Barnett, 2014; Nichols et al., 2012; Watson et al., 2011). The transportation and energy sectors are most likely to experience the greatest infrastructure impacts from severe winter storms. These sectors could expect short-term impacts from heavy snowfall, ice accumulations and strong winds, which could cause transportation delays and closures, tree and power line damage, roof collapse, and other structural damage. Winer severity also greatly affect the wildlife and ecosystems (e.g., Mech et al., 1988; Murphy et al., 2006l Dawe and Boutin, 2012; Delgiudice et al., 2013). For example, harsher winters will hamper the growth of trees in the following spring and summer (Galli et al., 1992). The winter weather can affect deer mortality, fawn production, and deer physical condition (including antler development) (Dawe and Boutin, 2012). Porter et al. (1983) found that severe winter conditions can reduce the egg hatching success of wild turkey. Winter mortality and impaired reproduction performance can result in a signficnat decline in the turkey population. Severe winters could also affect migration and contaminant accumulation in northern great lakes herring gulls (Hebert 1998) and the ratio of urea nitrogen to creatinine (nutritional restriction) of a free-ranging, generalist herbivore (Grace 2016). Therefore, it is important to monitor and understand the severity of winter. Awareness of winter severity may invoke protective or preventative measures to offset potential costs accumulated during higher severity.

The question of how “hard” a winter is for a given location depends on the climatological context, which relies on an objective characterization of winter severity. There are many methods to define the severity of winter. A winter severity index is an objective measure of the relative impact of winter weather. Previous studies of winter weather were often focused on event-specific quantities, such as snowstorms (e.g., Changnon et al. 2006; Kunkel et al., 2009; Lawrimore et al., 2014), snow cover (Brown and Robinson, 2011), precipitation types (Knowles et al., 2006; Feng and Hu, 2007), freezing degree-days (Assel 1980, 1998; Schummer et al., 2010; Johnson and Vrtiska, 2014), minimum temperature (Galli et al., 1992; Singh et al., 2016), or the combination of multiple quantities. Taken together, all of these elements could define the severity of a winter season, but they are incompatible in both their temporal and areal coverage. Some of these studies neglect some important aspects of a winter season, e.g., cumulative impact of winter duration, the occurrence of lighter snow events, and the effects of subfreezing temperatures.

The character of a winter can be defined by many of its features, including temperature averages and extremes, snowfall totals, snow depth, and the duration between onset and cessation of winter-weather conditions. To overcome weakness in the previous studies about the winter conditions, Boustead et al (2015) developed a winter season severity index (AWSSI) using widely available daily meteorological parameters to quantify the severity of a winter season, cumulative from the onset to the end of a given winter. AWSSI is calculated with a temperature component and a snow component, allowing an end-of-season total AWSSI to represent the severity of a season but also allowing a daily running calculation through a winter to track its severity. The temperature component uses maximum and minimum temperature data and is fairly straightforward. By contrast, the snow (precipitation) component is a little more complex. Snowfall and snow-depth data, if not available, can be estimated using daily temperature and precipitation. AWSSI is now use to

quantify the winter severity in the United States, and to trace a winter season in progress, placing it in the context of previous winters to ascertain its severity to date and to explore the range of outcomes of winters with similar severity to date (Boustead et al., 2015). However, none of the previous studies used this new index to quantify the winter conditions in other countries and for future projection.

This study used AWSSI to quantify the winter severity in the Southern Hemisphere (SH) during 1901-2012 using observational data and during 1950-2100 using the statistically downscaled CMIP5 simulations. We also analyzed the spatial and temporal variations of winter severity and its relationship to large-scale forcings, such as AAO and ENSO.

Work done and the results

2.1 Data and methods

The AWSSI blended the daily maximum and minimum temperature as well as the daily snowfall and snow depth to quantify the severity of winter. For a given day, the daily total AWSSI is determined on the basis of thresholds of maximum and minimum temperature, snowfall and snow depth. The criteria to determine daily points are listed in Table 1 (Boustead et al., 2015). These criteria are based on end-user input. After we obtained the daily points, then the severity of a given winter (or month) can be computed by summing the daily points for the winter (or month). As shown in Table 1, the AWSSI combined the impact of both temperature and snow. Therefore, the AWSSI can be determined as a temperature and snow components, termed as AWSSI_Temperature and AWSSI_Snow, respectively.

To compute the AWSSI for a given winter, the starting and end dates of a winter need to be determined. In conventional climate studies, the winter is usually defined as December to February in the Northern Hemisphere and June to August in the Southern Hemisphere. However, different regions have different climate, therefore using calendar months to determine winter ignore the regional characteristics of different climate regimes. The starting and end dates can be defined using different criterions, including the first and last frost dates (McCabe et al., 2015), the first and last snow covered dates (McCaffery and Maxell, 2010). These definitions usually only considered the impact of temperature or snow conditions and can only be used for specific research topics (e.g., agriculture and ecosystems).

Boustead et al (2015) outlined a series of criterions to define the start and ending date of winter. They argued that a combination of sensible weather conditions and calendar definition would best define a winter season. Specifically, the winter for a given region starts when the first of three conditions is met:

1) daily snowfall ≥0.1inch;

2) daily maximum temperature ≤ 32° F, or

3) it is 1 December in the Northern Hemisphere or June 1st in the Southern Hemisphere.

On the other hand, the cessation of winter for a given region can be determined when the last of the following four criterions is met:

1) daily snowfall ≥0.1 in. no longer occurs;

2) daily snow depth ≥0.1 in no longer occurs,

3) daily maximum temperature ≤32 °F no longer occurs, or

4) it is March 1st in the Northern Hemisphere or September 1st in the Southern Hemisphere.

Defining the winter severity need the temperature, and snowfall and snow depth data. However, there are no snowfall and snow depth data available in the SH. So it is necessary to estimate the snowfall and snow depth data when both data are unavailable or there are many missing data in snowfall and/or snow depth data. The snowfall and snow depth can be estimated using daily temperature and precipitation, as suggested by Fisk (2008), Bynn et al. (2008) and Trnka et al. (2010). Boustead et al. (2015) argued that the Fisk (2008) snowfall model is most applicable to estimate daily snowfall. This method first divides the daily temperature data into cold and mild conditions and the daily precipitation data into light, moderate and heavy categories (Table 2). Then the daily snowfall can be estimated based on different combination of temperature and precipitation categories (Table 3).

The Snow depth was estimated based on the degree-day method used in USDA (2004), which accounts the snowpack ablation, melting and compaction. The base temperature and melting factors are differed in different periods of the winter, which are shown in Table 4.

Both the existing snowpack and the daily snowfall are subject to an adjustment for decay. The compaction factor adjustment is given by

$$C_f=\exp(-0.08\times 0.2^{1/2}). \quad (1)$$

The snow depth is estimated as:

$$SD_n=SD_{n-1}C_f - C_m(T_{ave}-T_b) + SFnC_f \quad (2)$$

Where SDn is the snow depth on the day n, SDn-1 is the snow depth on the previous day, Cf is the compaction factor, Cm(˚F-1) is a degree-day coefficient (related to degree-days), Tave (˚F) is daily average temperature, Tb(˚F) is a base temperature. The Tb and Cm are given by Table 4.

Boustead et al. (2015) evaluated the above snowfall and snow depth model based on 52 weather stations in the US. They found that the snowfall and snow depth models are reasonable in estimating the snowfall and snow depth. However, it is not clear whether both models work well in different climate regimes. Therefore, this study used the daily temperature, precipitation, and snowfall and snow depth data from the U.S. Historical Climatology Network (USHCN, Easterling et al., 1999) during 1948-2015 to evlaute the snowfall and snow depth models. The USHCN data set contains 1221 cooperative stations that have high-quality long-term observations. These observational data have been subjected to quality control which includes homogeneity testing and adjustments to assure their reliability. To screen out the USHCN stations that have a large amount of missing values, the following three criteria were applied to each station. (1) If a winter month has missing precipitation (or snowfall and snow depth) observations for more than 5 days that month was removed from the analysis. (2) If a winter has missing precipitation (or snowfall and snow depth) observations for more than 10 days either clustered in one month or scattered in different months, that winter is considered having inadequate observations and was removed from the analysis. (3) Stations with less than 30 winters of adequate data during 1949–2015 were excluded from this study. This process retained 672 weather stations. We estimated the snowfall and snow depth using the aforementioned snowfall and snow depth models and then used the estimated values to calculate the AWSSI for the 672 stations, termed as precipitation-based AWSSI, or pAWSSI. Our results suggested that pAWSSI is a very good measure of AWSSI (detailed in section 2.2)

Besides the data in the U.S., we used the daily temperature and precipitation data developed for the Global Land Data Assimilation System (GLDAS) during 1901-2012 (Sheffield et al., 1996). This data covers the global land areas on 0.5-degree resolution. To evaluate the impact of climate changes on winter severity, the daily temperature and

precipitation from 21 CMIP5 models (Table 5) under RCP4.5 and RCP8.5 scenarios were statistically downscaled to 0.25-degree resolution. The daily temperature and precipitation in GLDAS and CMIP5 were subsequently used to calculate pAWSSI during 1901-2100.

2.2 Evaluating the precipitation-based AWSSI calculation

We firstly evaluated and modified the snowfall and snow depth models described by Boustead et al (2015) and calculated the snowfall and snow depth for the 672 USHCN weather stations. Then we used the estimated snowfall and snow depth as well as the daily temperature data to compute the pAWSSI (precipitation-based). We also calculated the AWSSI based merely on observed snowfall, snow depth and temperature. The pAWSSI and AWSSI are highly correlated (CC> 0.9) during 1948-2015, with a few exceptions (Figure 1). Because the correlation neglects the mean difference between pAWSSI and AWSSI, to overcome this limitation, we compute the consistent index (CI) (Willmott et al., 2012). The CI range from negative -∞ to 1.0. Usually, CI>0.0 indicates the estimated pAWSSI is good. The larger the CI, the closer the pAWSSI to AWSSI in terms of mean and variability. Figure 2 suggested that CI between pAWSSI and AWSSI is usually large than 0.8 in northern High Plains, southwest and southeast U.S. The CI is slightly weaker (0.6 to 0.8) in the south-central US and the Rocky Mountainous regions. Only a few locations in the Rocky Mountains with CI less than 0.6. Among all the 672 USHCN weather stations data analyzed, no stations with CI<0.5, suggesting that the pAWSSI is a very good estimation of AWSSI.

This notion is further supported by the long-term mean of pAWSSI and AWSSI (Figure 3). The spatial distribution of both indexes are resembled to each other. Both show lower values in the south US and west coastal regions, suggest mild winter there. The winter is most severe in the Rocky Mountains and Canada-US borders east of 90W. Additionally, the temporal variations of pAWSSI are nearly identical to that of the AWSSI (Figure 3).

These results suggested that it is reasonable to use merely daily temperature and precipitation to estimate the winter severity. Since the USHCN weather stations are homogeneously distributed and reflects different climate regimes (e.g., arid *vs* humid, mountainous regions *vs* prairies), suggesting that pAWSSI can also be applied to other counties, e.g., Eurasia and the SH.

2.3 Spatial and temporal variations of winter severity in Southern Hemisphere during 1901-2012.

The long-term average of pAWSSI in the SH based on GLDAS data is shown in Figure 4. As expected, the winter is most extreme in the Antarctica. There is no winter in the SH north of 30S except the Andes in the South America. The winter is pretty mild (pAWSSI< 70) in southern Africa and southeast Australia. In the southern South America (SSA) and New Zealand, the winter severity is moderate, except the Andes and over the mountainous regions in west New Zealand. Except the Antarctic, the AWSSI-snow is usually less than 10 points, suggesting that the contribution of snow to AWSSI is very small. This point is further supported by computing the ratio between AWSSI-temperature to AWSSI (shown in the bottom panel of Figure 4). It is clear that the temperature component contributed to more than 90% of the total AWSSI in most of the SH.

The long-term trend in pAWSSI are less robust and more spatially dependent in the SH. The pAWSSI in southern Africa, Australia, New Zealand and the coastal Antarctic is decreasing during 1901-2012 and 1951-2012 (Figures 5 and 6). The winter become more severe in majority of Antarctica, consistent with the cooling trend in this continent (Nicolas and Bromwich, 2014). The winter severity in the SSA show mixed results. Some regions show harsher winters while the other regions show more mild winters in this region (Figures

5 and 6). The pAWSSI-snow is increasing over most of Antarctica, consistent with increasing snowfall in the high latitudes in a warmer climate.

We further evaluated the spatial variations of pAWSSI in SSA using EOF method. We focused on SSA mainly because 1) the AWSSI does not work well in regions with permeant ice cover (Boustead et al., 2015) and 2) winter is more severe and wide spread in SSA compared to other regions in the middle latitude SH. The first three EOF modes and their principal components (PCs) are shown in Figures 7 and 8. The first EOF mode (EOF1) show simultaneous variations over SSA (Figure 7). The second EOF mode (EOF2) show a north-south see-saw pattern, whereas the third EOF mode (EOF3) shows opposite variations between regions around 40S and the subtropics and the south Argentina. The PCs associated with EOF1 and EOF2 (PC1 and PC2) show considerable interannual variations, while the PC3 show obvious decreasing trend (Figure 8). The PC1 is closely linked to SST in the eastern tropical Pacific Ocean, associated with ENSO (Figure 9). A La Nina condition may lead to cool temperature in SSA and hence higher AWSSI. The PC3 is closely related a warming in the ocean, especially over the tropical and Southern Ocean (Figure 9). We also analyze the EOF modes of temperature and snow component of winter severity in SSA. The EOF modes of temperature-AWSSI is very similar to that of the pAWSSI (Figure 10 vs Figure 7), consistent with the facts tht the AWSSI is dominated by temperature changes in the Southern Hemisphere (Figure 4). The EOF modes of the snow component of winter severity in SSA is less organized as the temperature component (Figure 11), possibly because 1) the snowfall and snow cover in SSA is scarce and 2) the variations of snowfall and snow depth are less spatially coherence compared to temperature.

To examine the impact of large scale forcings (e.g., ENSO and AAO) and the winter severity in the SH, we correlated the ENSO and AAO with the pAWSSI during 1902-2012. The impact of June-August AAO on pAWSSI is overall positive in the Antarctica and

negative over the mid-latitude SH (Figure 12), consistent with the out-of-phase relationship in atmospheric circulation between the south pole and the mid-latitude SH. However, the AAO signature shows distinct regional patterns. The AAO is significantly correlated to pAWSSI in SSA and south Africa, especially the temperature based AWSSI (AWSSI_temperature). The AAO impact on snow (AWSSI snow) is much weaker. In some regions, the impact of AAO on snow and temperature are opposite to each other. For example, the AAO is negatively and significantly correlated to the AWSSI_temperature in the Antarctic Peninsula. However, the AAO is positively and significantly correlated to AWSSI_snow in this region. Therefore, the AAO on the pAWSSI is overall weak in Antarctic Peninsula due to opposite impact of AAO on temperature and snow.

The ENSO can also strongly influence the winter severity in the Southern Hemisphere (Welhouse et al., 2016). The June-August Nino 3.4 SST is positively correlated to pAWSSI in Australia and New Zealand, but negatively correlated to pAWSSI in SSA (Figure 13). The ENSO impact on SSA is most obvious on temperature (AWSSI_temperature). The ENSO impact on snow is pretty weak (Figure 13). These results are consistent to the EOF analysis over SSA (Figures 7-9).

2.4 Projected future changes in winter severity in the Southern Hemisphere

The long-term mean pAWSSI during 1971-2000 calculated based on the 21 CMIP5 models are shown in Figure 14. The spatial distribution of pAWSSI and the contribution of snow and temperature to AWSSI as well as the ratio of AWSSI_temperature to AWSSI are all resembled the GLDAS (Figure 4 vs Figure 14), suggesting that the ensemble of the 21 CMIP5 models did a very good job in simulating the observed winter severity.

The projected changes in pAWSSI for the middle and late of this century derived from the model simulations by the 21 CMIP5 models under scenarios RCP45 and RCP8.5 are shown in Figures 15-18. Less severe winters are projected over the entire SH. The most noticeable changes are projected over the mid-latitude SH. Under RCP4.5, the pAWSSI is projected to decrease about 30-50% in SSA, 50-60% in southern Africa and 40-50% in Australia and New Zealand by the end of this century. In Antarctica, the projected changes in pAWSSI is weak, with majority of Antarctica show less 10% decrease in winter severity. The winter severity due to snow and temperature are also analyzed. The AWSSI due to snow is projected to decrease 60-90% in SSA. However, the AWSSI_snow is projected to increase 10-20% in most Antarctica (Figure 17). This results are consistent with projected increase in precipitation (snowfall) in high latitudes due to global warming (e.g., Feng et al., 2014). On the contrary, the AWSSI due to temperature is projected to decrease 10-20% under RCP4.5 by the end of this century. Because the AWSSI_temperature overwhelmed the mean pAWSSI (Figures 4 and 14), the weak decrease in AWSSI_tempeature are still stronger than the increase in AWSSI_snow, leading to decreasing pAWSSI (weaker winter severity) everywhere in the SH.

The projected changes in winter severity under RCP8.5 is similar to that of RCP4.5, except the magnitude is larger (Figures 16 and 18). For example, the pAWSSI is projected to decrease 60-90% in SSA, 70-90% in southern Africa and 70-80% in Australia and New Zealand under RCP8.5 by the end of this century. The winter severity is projected to decrease 10-20% in the Antarctica. The winter severity due to snow is projected to decrease 80-90% in SSA, but increase 10-30% over most Antarctica. In some locations in the Antarctica, the AWSSI_snow if projected to increase 50%. On the contrary, the winter severity due to temperature is projected to decrease more than 70% in the middle latitude SH and 10-30% in the Antarctica.

We also plotted the temporal variations of pAWSSI and its temperature and snow components averaged over South America, South Africa, Antarctica as well as Australia and New Zealand using GLADS and the ensemble of the 21st CMIP5 models during 1901-2100 (Figures 19-21). During the 1951-2005 (the overlapping period of GLDAS and the model), the model did a very good job in simulating the temporal variations of AWSSI and the temperature component of AWSSI over the four continents. The models also captured the long-term trend of AWSSI_snow, but underestimated the decadal variations in GLDAS. These discrepancies may be caused by model deficiencies, uncertainties in natural and anthropogenic forcings, unknown model initial conditions (Feng and Fu, 2013; Feng et al., 2014). The projected changes in winter severity in each continents during the middle and end of this century are summarized in Figures 22-24. The median and the spread of the 21 CMIP5 models simulations are also shown in these figures.

3 Future work

Future work will focus on further evaluation of the snowfall and snow depth models as well as the AWSSI based merely on temperature and precipitation. There snow depth data in Eurasia (e.g., Russia, Mongolia and China) on hundreds of weather stations are currently became available, which can be used to evaluate the snow depth model. We can also compare the snow cover areal extent over based on weather stations and satellite over the Northern Hemisphere with the snow depth data estimated by temperature and precipitation. There are no snowfall and snow depth data available in the SH, but the snow cover can be retrieved from satellite images. Therefore, it is critically need to evaluate and hence modify the

snowfall and snow depth models to better simulate both quantities and then subsequently use them to quantify the winter severity.

References

Abram et al. (2013). Accerleration of snow melt in Antarctic Peninsula ice core during the twentieth century. Nature Geoscience, 6, DOI: 10.1038/NGEO1787.

Andrey J., B. Mills, M. Leahy and J. Suggett (2003). Weather as a chronic hazard for road transportation in Canadian Cities. Natural Hazards, 28, 319-343.

Assel, R. A., (1980). Maximum freezing degree-days as a winter severity index for the Great Lakes, 1897–1977. Mon. Wea. Rev., 108, 1440–1445.

Assel, R. A., (1998). The 1997 ENSO event and implication for North American Laurentian Great Lakes winter severity and ice cover. Geophysical Res. Lett., 25, 1031-1033.

Bromwich D. H. et al. (2013). Central West Antarctica among the most rapidly warming regions on Earth. Nature Geoscience, 6, 139-145.

Boustead B. E. M et al. (2015). The accumulate winter season severity index. J. Applied Meteol. Climatol., 54, 1693-1712.

Brown R.D, D.A. Robinson (2011). Northern Hemisphere spring snow cover variability and change over 1922–2010 including an assessment of uncertainty. The Cryosphere, 5, 219-229.

Byun, Kun-Young, Jun Yang, and Tae-Young Lee. (2008). A snow-ratio equation and its application to numerical snowfall prediction. *Weather and Forecasting* 23, 644-658.

Changnon S. A. (1979). How a severe winter impats on individuals. Bull. Ameri. Meteorol. Soc., 60, 110-114.

Changnon, D., C. Merinsky, and M. Lawson (2008), Climatology of surface cyclone tracks associated with large central and eastern U.S. snowstorms, 1950–2000. Mon. Wea. Rev.,

136, 3193–3202.

Changnon, DD. Changnon, and T. R. Karl, 2006: Temporal and spatial characteristics of snowstorms in the contiguous United States. J. Appl. Meteor. Climatol., 45, 1141–1155.

Dawe K. L. and S. Boutin (2012). Winter severity index using widely available weather information. *Wildlife Research* 39, 321-328.

Delgiudice G. D., B. A Sampson and J. H. Giudice (2013). A long-term assessment of the effect of winter severity on the food habits of white-tailed deer: Winter Food Habits of Northern Deer. The Journal of Wildlife Management 77, 1664–1675.

Easterling, D. R., T. R. Karl, J. H. Lawrimore, and S. A. Del Greco (1999), United States historical climatology network daily temperature, precipitation, and snow data for 1871–1997, *ORNL/CDIAC-118, NDP-070*, 84 pp., Carbon Dioxide Inf. Anal. Cent., Oak Ridge Natl. Lab., Oak Ridge, Tenn.

Feng S. and Q. Hu (2007). Changes in winter snowfall/precipitation ratio in the contiguous United States. J. Geophys. Res, 112:D15109.

Feng S. and Q. Fu (2013). Expansion of global drylands under a warming climate. *Atmos. Chem. Phys.* 13, 10084-10094.

Feng S., Q. Hu, F. Chen, C.-H. Ho, R. Li and Z. Tang (2014). Projected climate shift under future global warming from multi-model, multi-scenario, CMIP5 simulations. *Global and Planetary Change*, **112**, 41-52.

Galli M., M. Guadalupi, T. Nanni, L. Ruggiero and F. Zuanni (1992). Ravenna pine trees as monitors of winter severity in N-E Italy. Theoretical and Applied Climatology, 45, 217-224.

Grace P. L., et al. (2016). The influence of plant defensive chemicals, diet composition, and winter severity on the nutritional condition of a free-ranging, generalist herbivore. Oikos

Hebert, C E (1998). Winter severity affects migration and contaminant accumulation in northern Great Lakes herring gulls." *Ecological Applications* 8, 669-679.

Huang C. and A. Barnett (2014). Human impacts: winter weather and health. Nature Climate Change, 4, 173-174.

Johnson H.M. and M. P. Vrtiska (2014). Weather variables affecting Canada Goose Harvest in Nebraska. Great Plains Research, 24, 135-152.

Knowles, N., M. D. Dettinger, and D. R. Cayan (2006), Trends in snowfall versus rainfall in the western United States, *J. Clim.*, **19**, 4545–4559.

Kunkel K. E. et al. (2009). Trends in twentieth-century U.S. snowfall using a quality-controlled dataset. J. Atmos. Oceanic Technology, 26, 33-44.

Lawrimore J et al. (2014). Trends and variability in severe snowstorms east of the Rocky Mountains. J. Hydrometeorology, 15, 1762-1777.

Mansikkaniemi H, (1979). Index of winter severity and its regional variation in Finland. International Journal of Geography, 157, 75-87.

McCabe G.J., J. L. Betancourt and S. Feng (2015). Variability in the start, end, and length of frost-free periods across the conterminous United States during the past century. Int. J. Climatol., DOI: 10.1002/joc.4315.

McCaffery R. M. and B. A. Maxell (2010). Decreased winter severity increases viability of a montane frog population.PNAS, 107, 8644–8649.

Mech D., S. H. Fritts and W. J. Paul (1988). Relationship between winter severity and wolf depredations and domestic animals in Minnesta. Wildl. Soc. Bull., 16, 269-272.

Murphy M.H., M. J. Connerton and D. J. Stewart (2006) Evaluation of Winter Severity on Growth of Young-of-the-Year Atlantic Salmon, Transactions of the American Fisheries Society, 135:2, 420-430.

Nicolas J. P. and D. H. Bromwich (2014). New reconstruction of Antarctic near-surface

temperatures: multidecadal trends and reliability of global reanalysis. J. Climate, 27, 8070-8093.

Nichols R. B., W. F. McIntyre, S. Chan, D. Scogstad-Stubbs, W. M. Hopman and A. Baranchuk (2012). Snow-shoveling and the risk of acute coronary syndromes. Clinical Research in Cardiology, 101, 11-15.

Rauber R.M., J. E. Walsh and D. J. Charlevoix (2013). Server and hazardous weather: an introduction to high impact meteorology. Kendall Hunt publishing company, 612pp.

Schummer, M. L., R. M. Kaminski, A. H. Raedeke, and D. A. Graber, 2010: Weather-related indices of autumn–winter dabbling duck abundance in middle North America. J. Wildl. Manage., 74, 94–101.

Sheffield, J., Goteti, G., and Wood, E. F.: Development of a 50-yr high-resolution global dataset of meteorological forcings for land surface modeling, J. Clim., 19, 3088–3111, 2006.

Watson, D., B. Shields, and G. Smith, (2011). Snow shovel–related injuries and medical emergencies treated in US EDs, 1990 to 2006. American Journal of Emergency Medicine, 2911-17. doi: 10.1016/j.ajem.2009.07.003.

Welhouse L. J et al. (2016). Composite analysis of the effect of ENSO events on Antarctica. J. Climate, 29, 1797-1808.

Willmott, C.J., S.M. Robeson, and K. Matsuura (2012). A refined index of model performance. International Journal of Climatology, 32, 2088-2094.

Table 1: Points contributions to daily AWSSI based on daily maximum and minimum temperature, snowfall and snow depth (Boustead et al., 2015).

	Temperature (°F)		Snow (in.)	
Points	Max	Min	Fall	Depth
1	25–32	25–32	0.1–0.9	1
2	20–24	20–24	1.0–1.9	2
3	15–19	15–19	2.0–2.9	3
4	10–14	10–14	3.0–3.9	4–5
5	5–9	5–9	—	6–8
6	0–4	0–4	4.0–4.9	9–11
7	From −1 to −5	From −1 to −5	5.0–5.9	12–14
8	From −6 to −10	From −6 to −10	—	15–17
9	From −11 to −15	From −11 to −15	6.0–6.9	18–23
10	From −16 to −20	From −16 to −20	7.0–7.0	24–35
11	—	From −20 to −25	—	—
12	—	—	8.0–8.9	—
13	—	—	9.0–9.9	—
14	—	—	10.0–11.9	—
15	<−20	From −26 to −35	—	≥36
18	—	—	12.0–14.9	—
20	—	<−35	—	—
22	—	—	15.0–17.9	—
26	—	—	18.0–23.9	—
36	—	—	24.0–29.9	—
45	—	—	≥30.0	—

Table 2. Different categories of daily temperature and daily precipitation used to estimate the daily snowfall.

Temperature (unit ˚F)		Precipitation (unit inches)			
Cold	Mild	Light	Moderate	Heavy	
				Heavy-1	Heavy-2
≤27.5	> 27.5	0.01≤P≤0.06	0.06<P≤0.42.	0.42<P≤1.49	P>1.49

Table 3. Daily proxy snowfall formula. Where T_{avg}, T_{max}, and T_{min} are daily average, maximum and mean temperature. The "SF" is the daily snowfall.

		Cold	Mild
Light		$SF=0.259+15.413P-0.007(T_{avg}+20)$	$SF=0.551+5.017P-0.014\ T_{max}$
Moderate		$SF=2.081+12.331P-0.031(T_{avg}+20)-0.186(T_{max}-T_{min})^{1/2}$	$SF=-3.563+4.346P^{1/2}+3969.927T_{max}^{-2}$
Heavy	Heavy-1	$SF=19.237+7.266P-0.346(T_{avg}+20)-0.245(T_{max}-T_{min})-3.3$	$SF=-3.563+4.346P^{1/2}+3969.927T_{max}^{-2}$
	Heavy-2	$SF=19.237+7.266P-0.346(T_{avg}+20)-0.245(T_{max}-T_{min})-3.8$	

Table 4. Seasonally varying melting factors for snow melting rate and the base temperature (T_b) for calculating the degree-day.

Period	T_b	C_m
Up to 1 December	32	0.30
1 Dec-15 Jan	25	0.25
16 Jan-9 Feb	23	0.25
10 Feb-6 Mar	30	0.25
7 Mar-end	30	0.25

Table 5: A list of CMIP5 GCMs used in this study with a brief description. The daily temperature and precipitation during 1950-2100 from these models were statically downscaled to quarter-degree resolution. The data during 1950-2005 are based on historical run, while during 2006-2100 are based on RCP4.5 and RCP8.5 scenarios, respectively.

	Model name	Resolution (lon by lat)	Origin
1	ACCESS1.0	1.875×1.25	Commonwealth Scientific and Industrial Research Organization (CSIRO), Australia
2	BCC-CSM1.1	2.815×2.815	Beijing Climate Center, China
3	BNU-ESM	2.8125×2.8125	Beijing Normal University,China
4	CanESM2	2.815×2.815	Canadian Centre for Climate, Canada
5	CCSM4	1.25×0.9	National Center for Atmospheric Research, USA
6	CESM1-BGC	1.25×0.9	National Center for Atmospheric Research, USA
7	CNRM-CM5	1.40×1.40	Centre National de Recherches Meteorologiques, France
8	CSIRO-Mk3.6	1.875×1.875	Commonwealth Scientific and Industrial Research, Australia
9	GFDL-CM3	2.5×2.0	Geophysical Fluid Dynamics Laboratory, USA
10	GFDL-ESM2G	2.5×2.0	Geophysical Fluid Dynamics Laboratory, USA
11	GFDL-ESM2M	2.5×2.0	Geophysical Fluid Dynamics Laboratory, USA
12	INM-CM4	2.0×1.5	Institute for Numerical Mathematics, Russia
13	IPSL-CM5A-LR	3.75×1.875	Institut Pierre-Simon Laplace, France
14	IPSL-CM5A-MR	2.5×1.25	Institut Pierre-Simon Laplace, France
15	MIROC5	1.40×1.40	Atmosphere and Ocean Research Institute, Japan
16	MIROC-ESM	2.815×2.815	Japan Agency for Marine-Earth Science and Technology, Japan
17	MIROC-ESM-CHEM	2.815x2.815	Japan Agency for Marine-Earth Science and Technology, Japan
18	MPI-ESM-LR	1.875×1.875	Max Planck Institute for Meteorology, Germany
19	MPI-ESM-MR	1.875×1.875	Max Planck Institute for Meteorology, Germany
20	MRI-CGCM3	1.125×1.125	Meteorological Research Institute, Japan
21	NorESM1-M	2.5×1.875	Norwegian Climate Centre, Norway

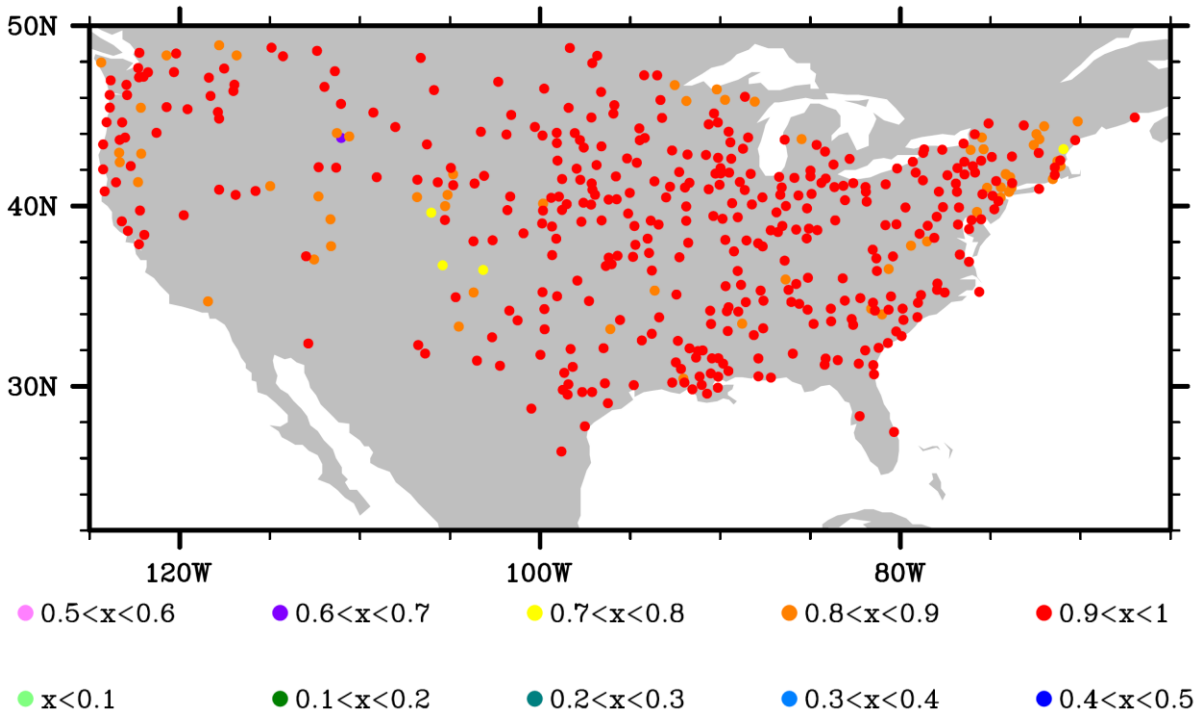

Figure 1: Correlation between AWSSI and pAWSSI during 1948-2015 based on 672 stations in USHCN.

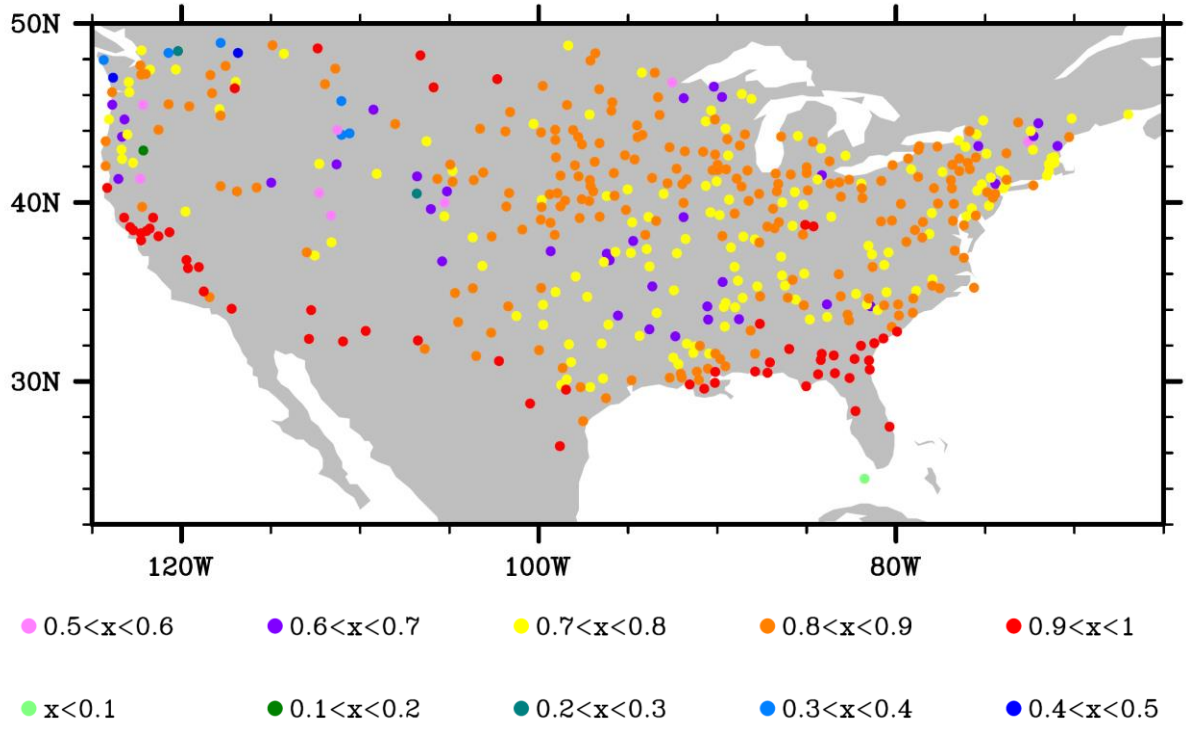

Figure 2. The spatial distribution of consistent index between pAWSSI and AWSSI during 1948-2015.

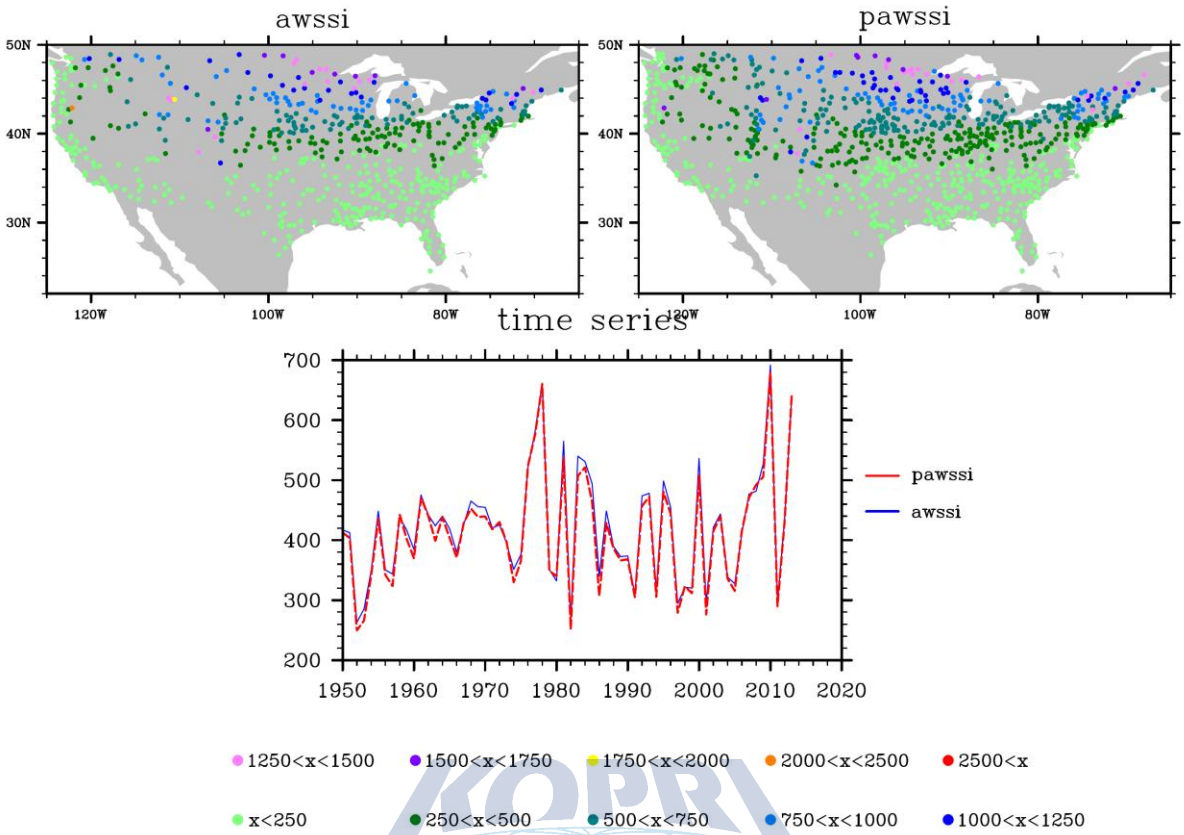

Figure 3: The spatial distribution of long-term climatology (1948-2015) of AWSSI (upper left) and pAWSSI (upper right) in the continental United States. Bottom: the temporal variation of the AWSSI and pAWSSI averaged over the continental United States.

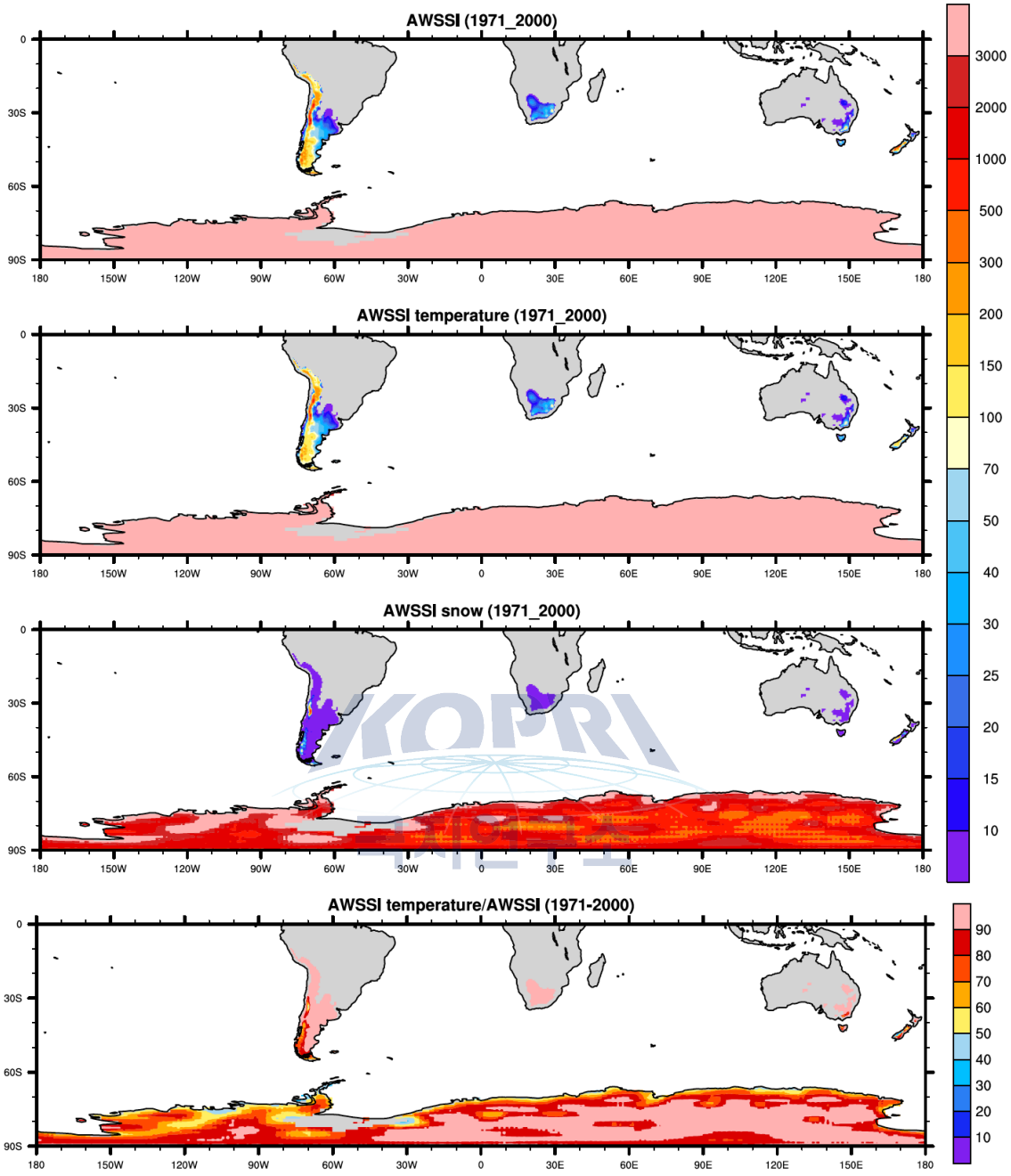

Figure 4: The long-term climatology of pAWSSI (upper panel), pAWSSI temperature component (2nd panel), pAWSSI snow component (3rd panel) during 1970-2000 based on GLDAS data. The ratio between pAWSSI temperature to pAWSSI is shown in the 4th panel.

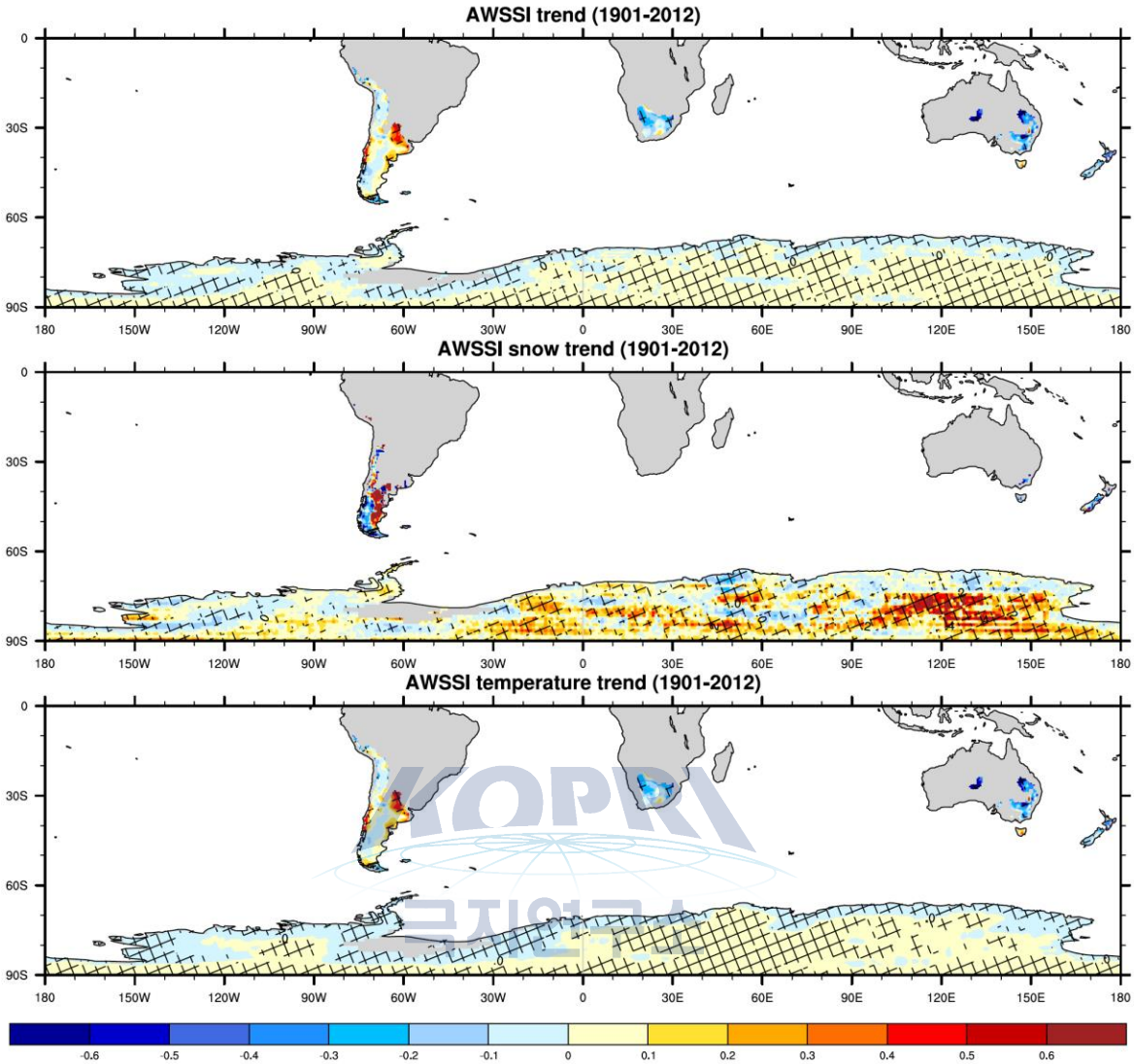

Figure 5: The linear trend in pAWSSI (upper panel), pAWSSI snow (middle panel) and temperature (lower panel) components during 1901-2012. The regions with significant trend (95% confidence level) are hatched. The unit is %/year.

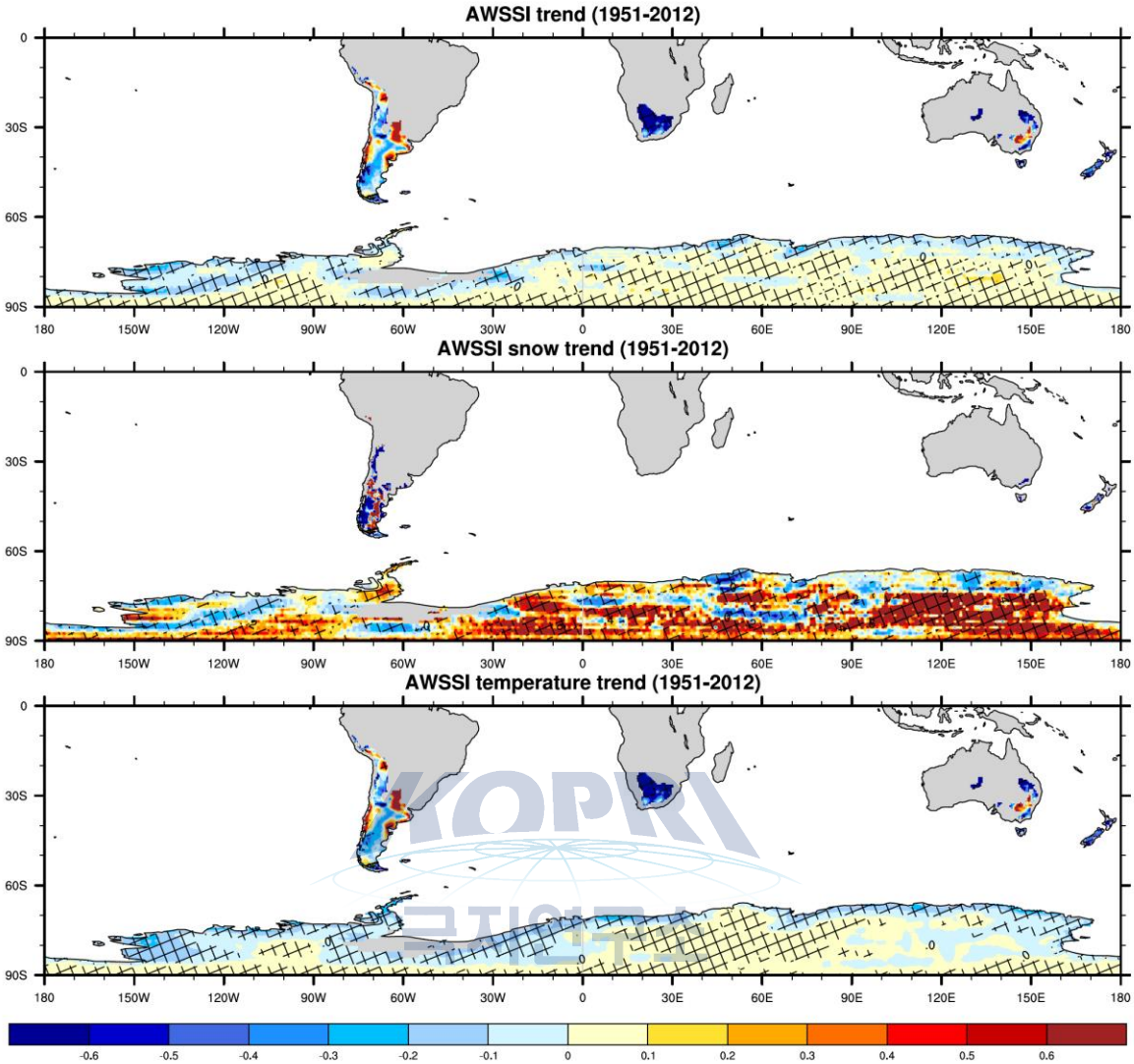

Figure 6: Same as Figure 5, except for 1951-2012, when the data are more reliable.

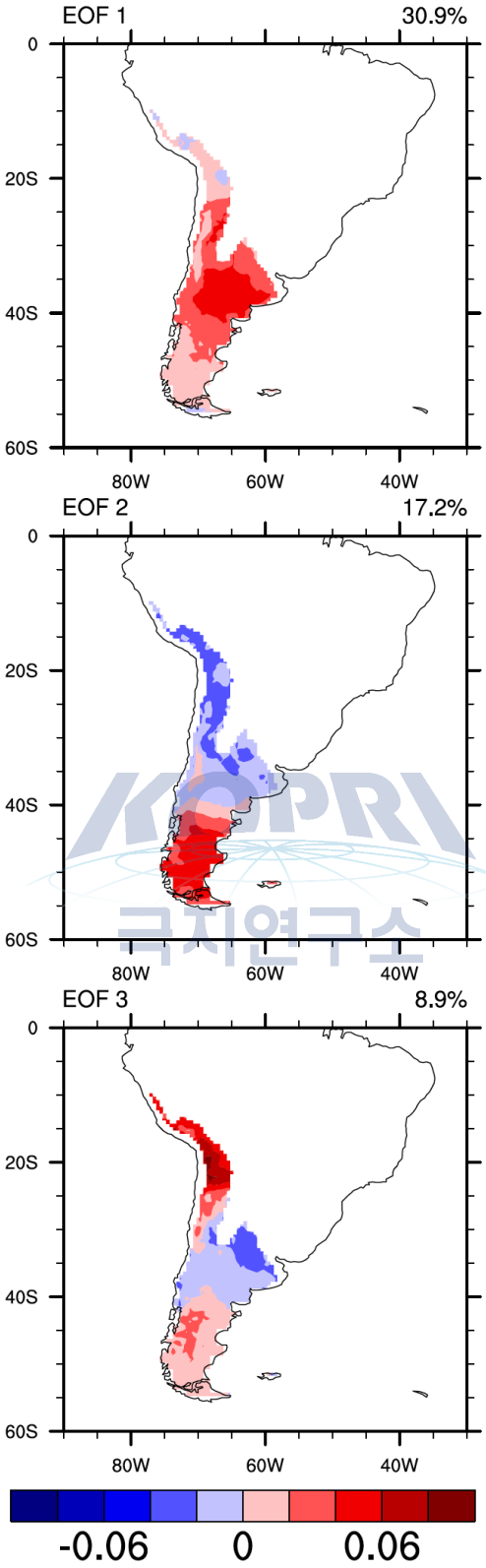

Figure 7: The EOF modes of pAWSSI in southern South America during 1901-2012. The data are based on GLDAS data.

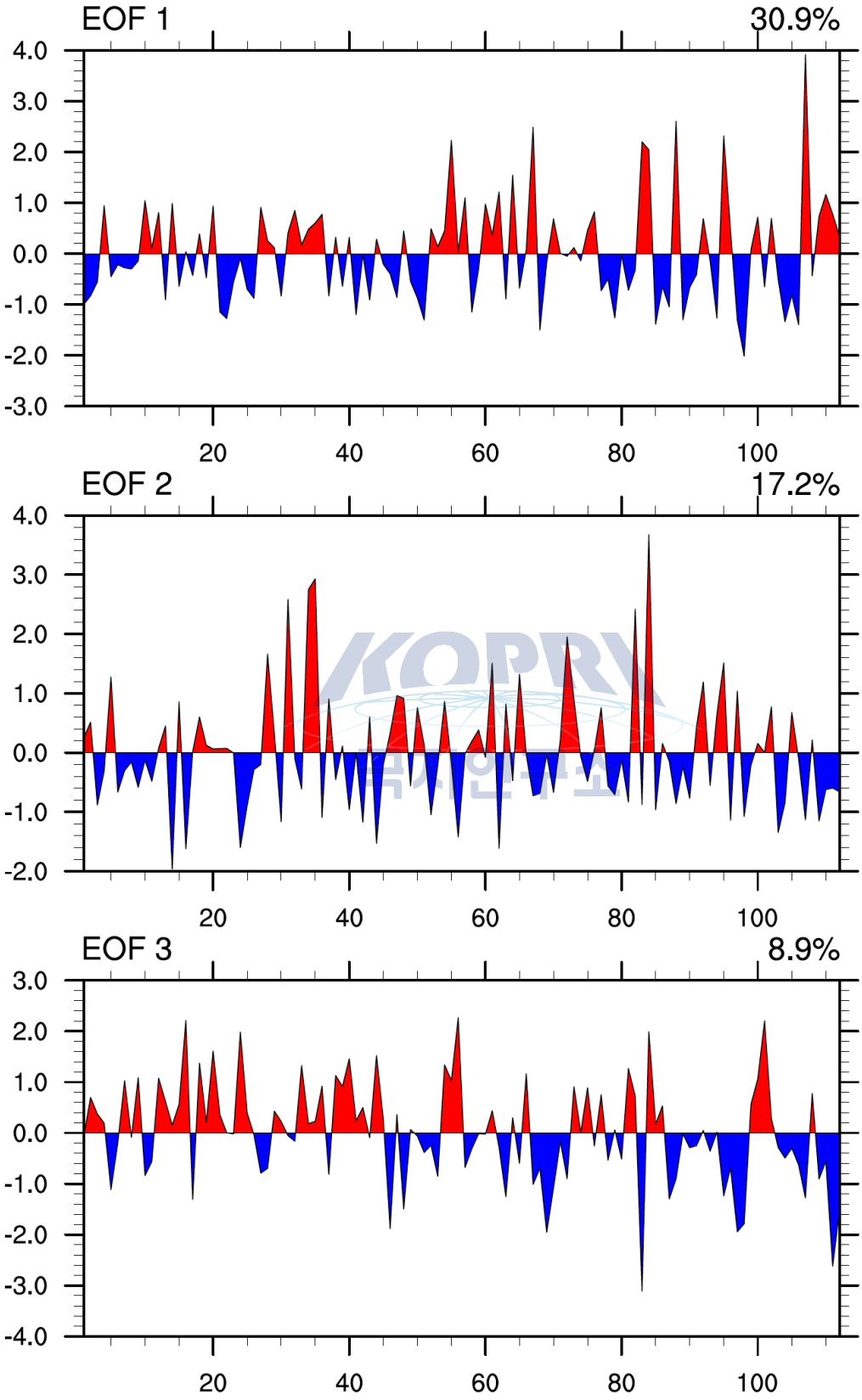

Figure 8: The temporal variations of the principal components of the pAWSSI in the southern South America.

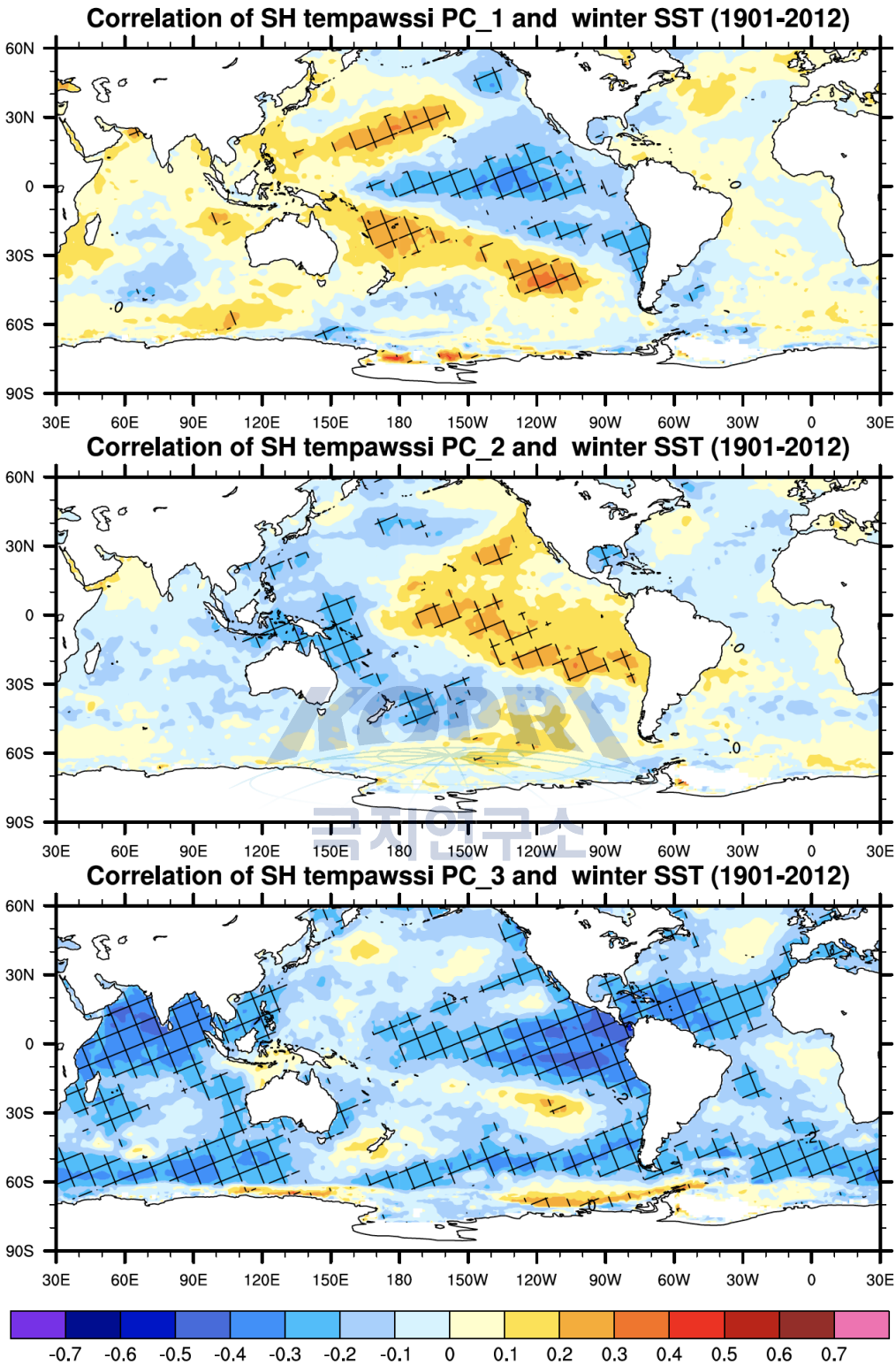

Figure 9: Correlations between the pAWSSI PCs in the southern South America and the southern winter (June-August) SST during 1901-2012. Hatched areas indicate the correlations are significant at 95% confidence level.

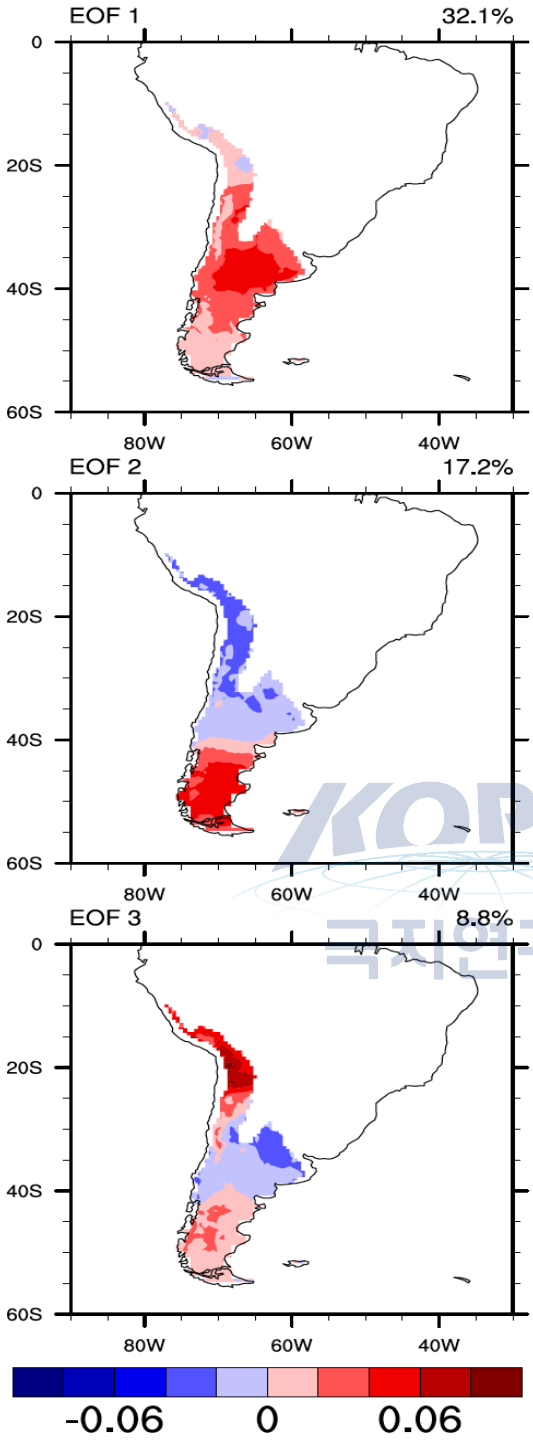

Fig.10. Same as Figure 7 but for the pAWSSI_temperature

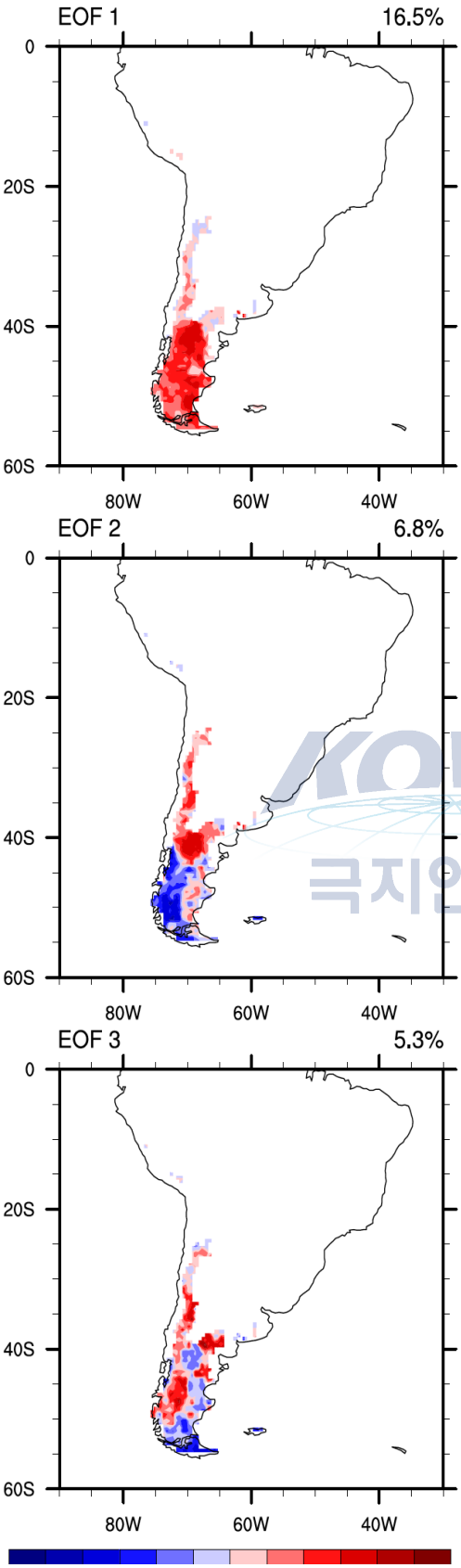

Fig.11. Same as Figure 7 but for the pAWSSI_snow

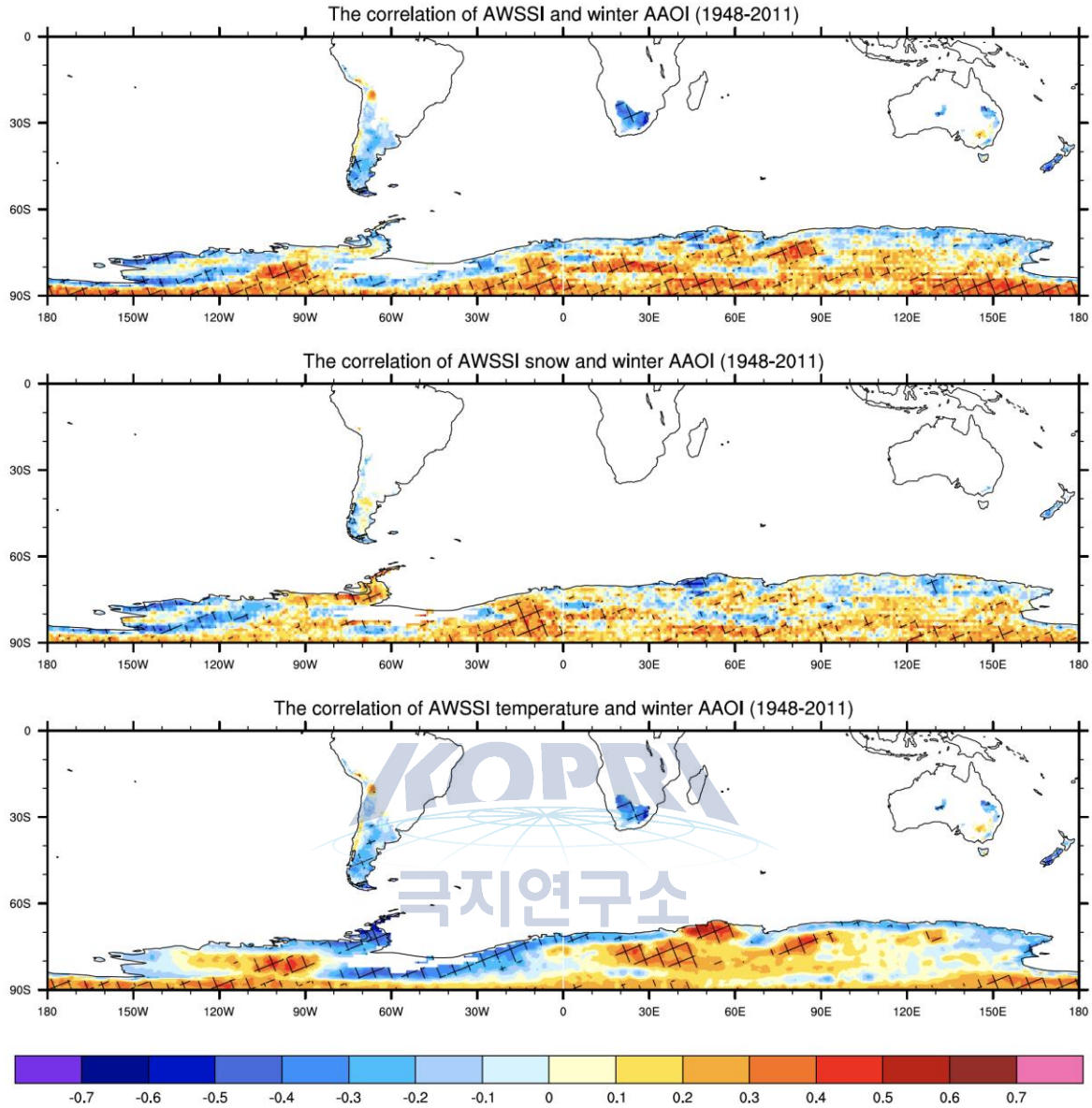

Figure 12: Correlations between southern winter (June-August) AAO and the pAWSSI (upper panel), pAWSSI snow (middle panel) and pAWSSI temperature (lower panel) in the Southern Hemisphere during 1948-2011. Hatched areas indicate the correlations are significant at 95% confidence level.

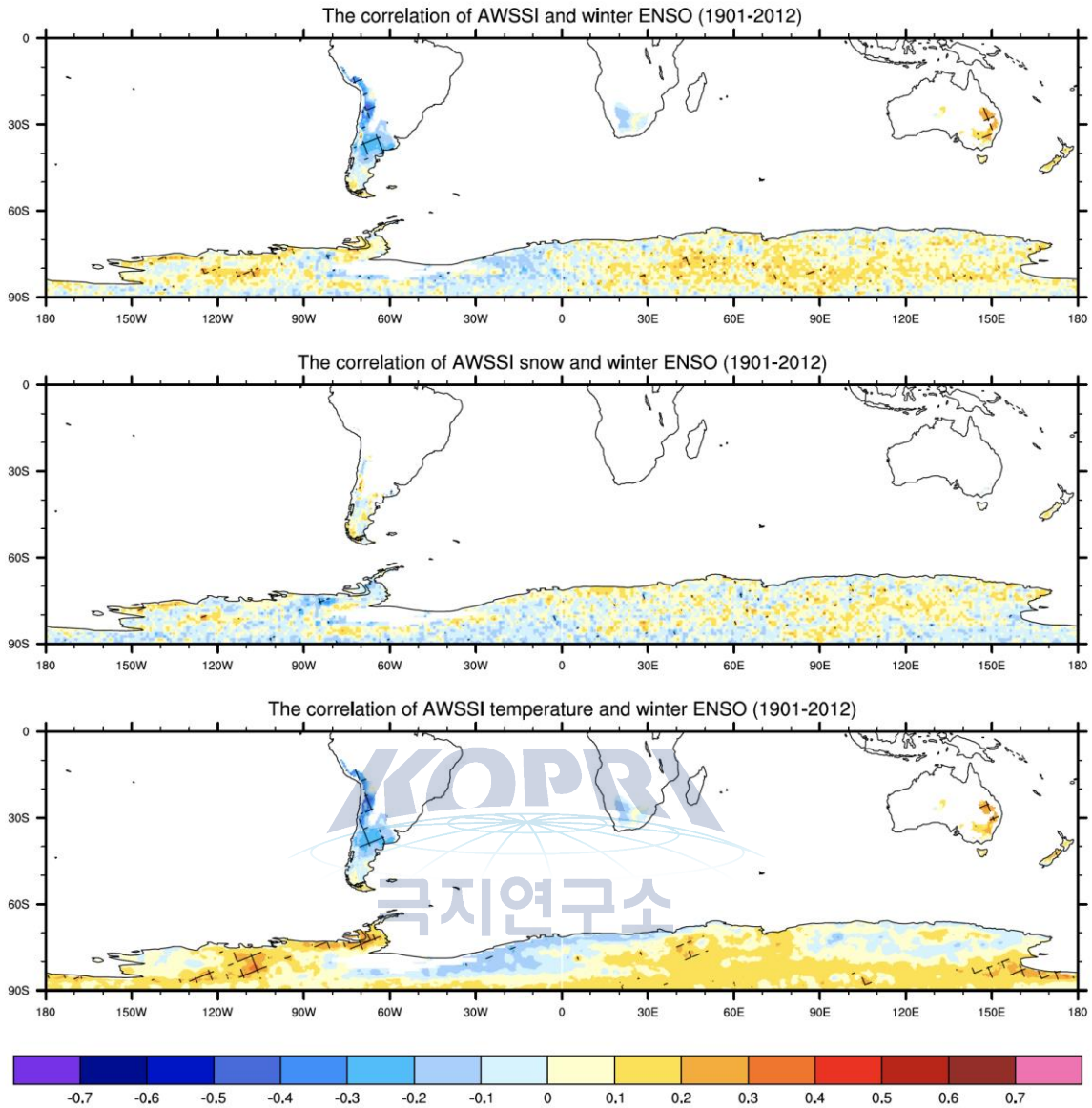

Figure 13: Same as Figure 12, but for the southern winter (June-August) Nino 3.4 SST during 1901-2012.

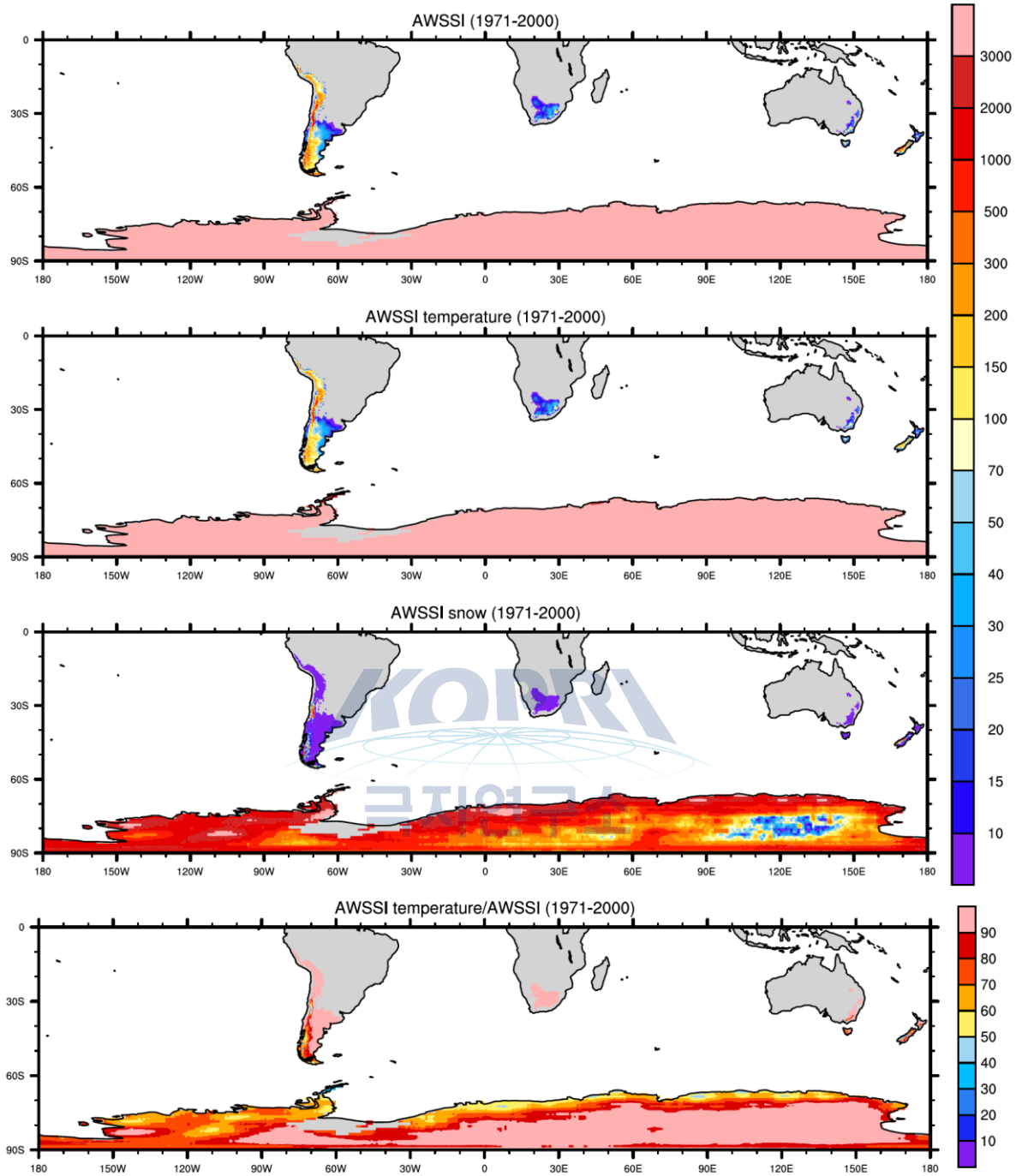

Figure 14: Same as Figure 4, but based on the ensemble of 21 CMIP5 models. The modeled data are statistically downloaded to quarter-degree resolution.

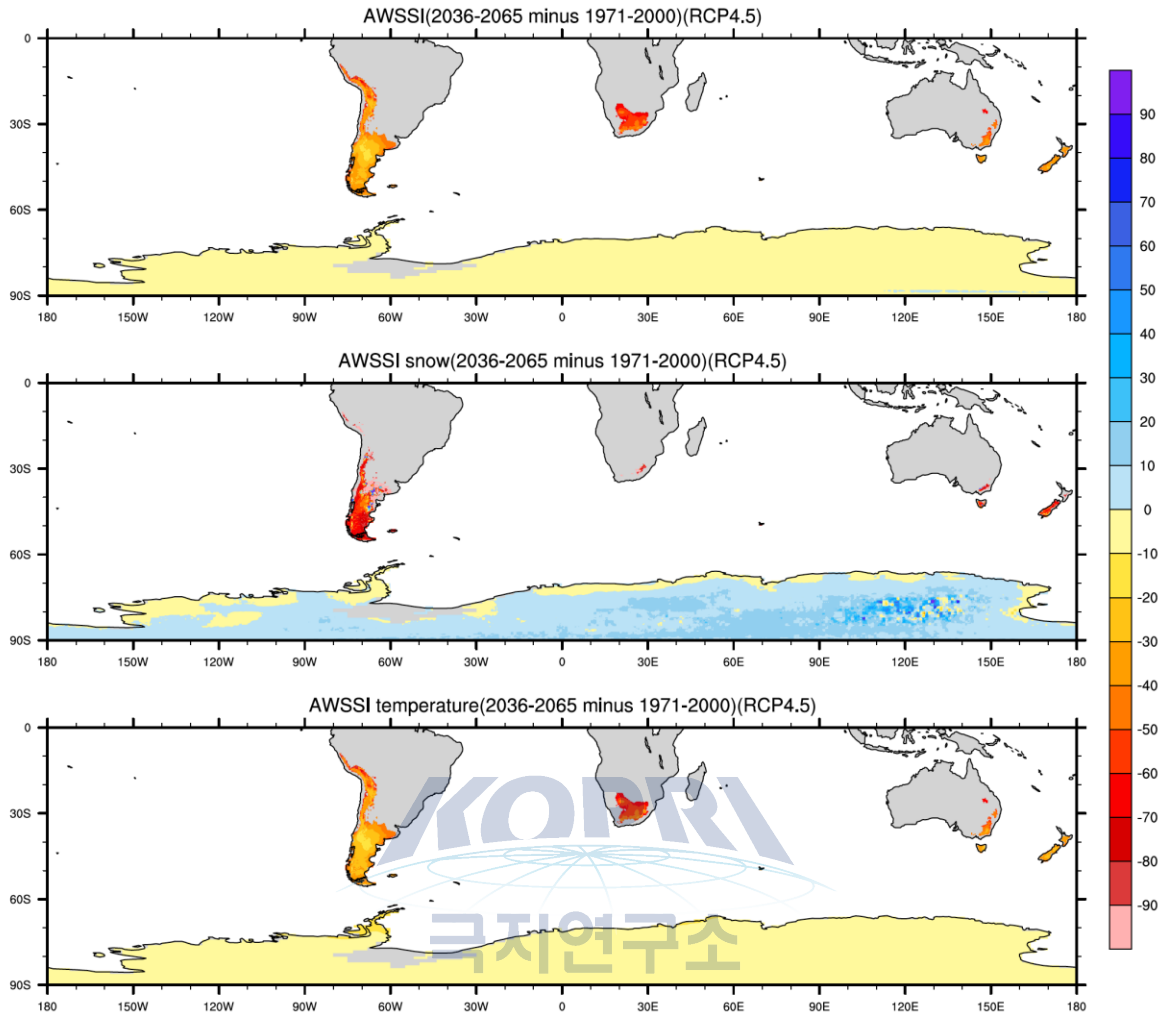

Figure 15: Spatial distribution of the projected changes (%) in pAWSSI (upper panel), pAWSSI snow (middle panel) and pAWSSI temperature (lower panel) between 2036-2065 and 1971-2000 under the RCP4.5 scenario.

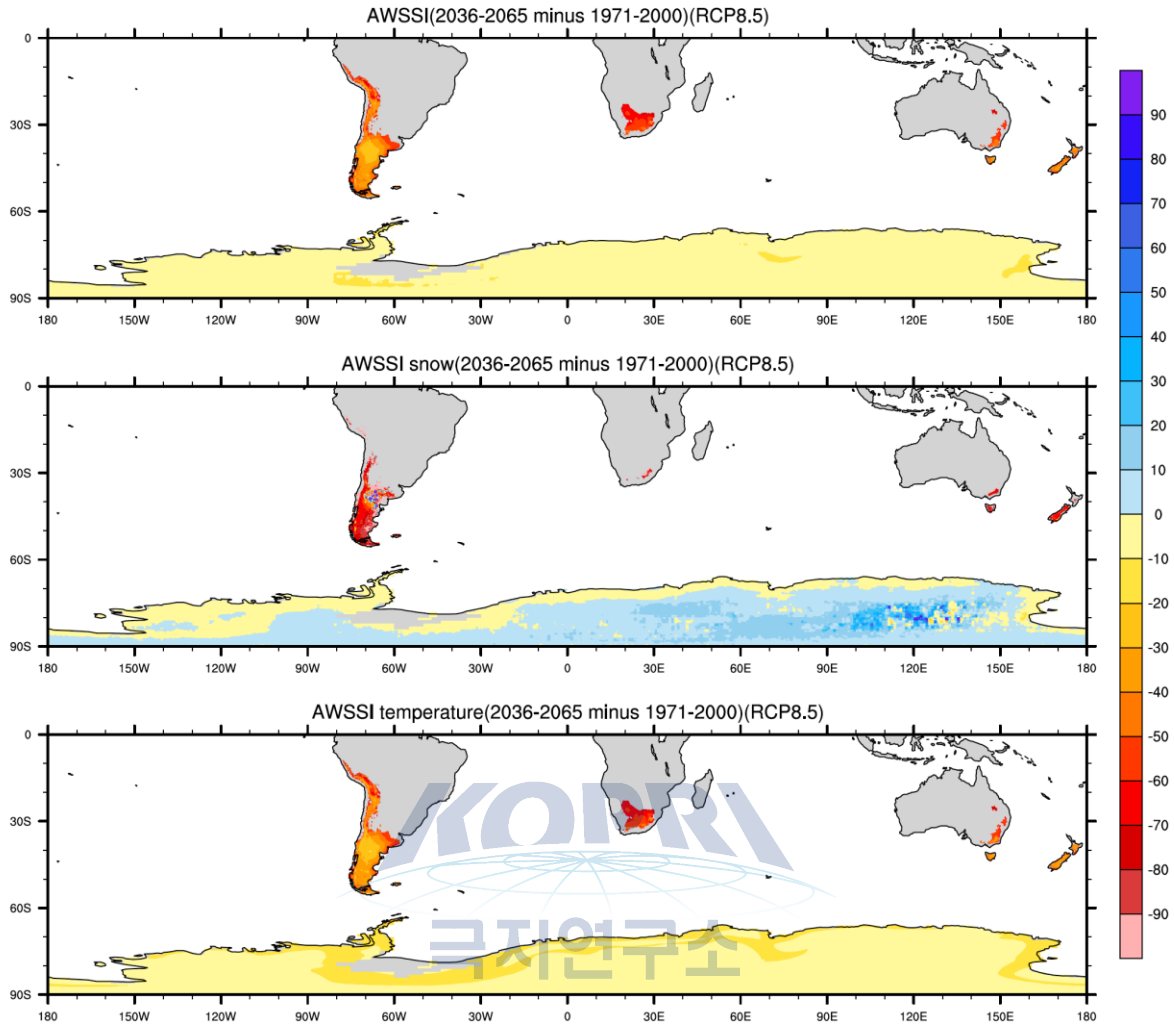

Figure 16: Spatial distribution of the projected changes (%) in pAWSSI (upper panel), pAWSSI snow (middle panel) and pAWSSI temperature (lower panel) between 2036-2065 and 1971-2000 under the RCP8.5 scenario.

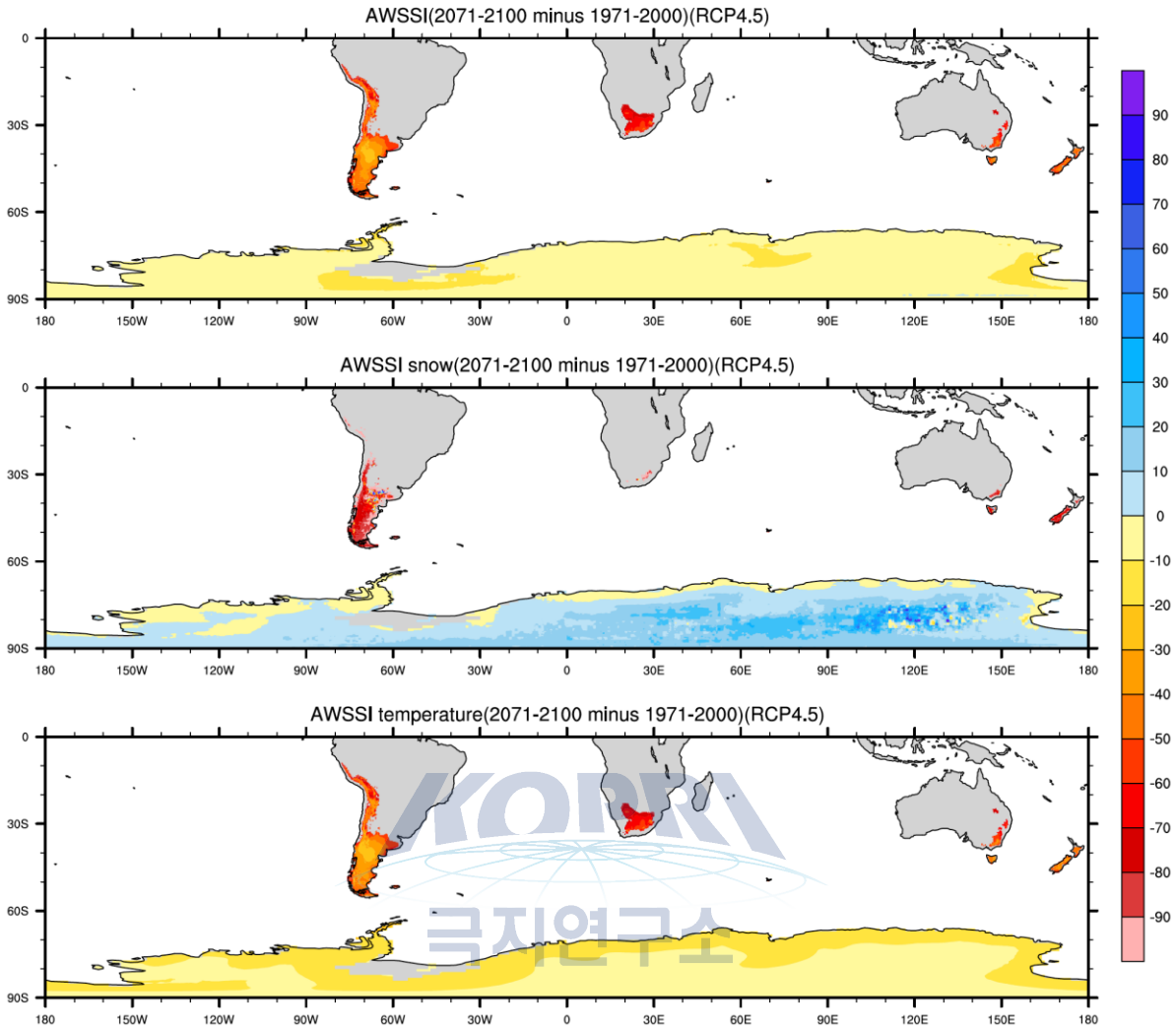

Figure 17: Spatial distribution of the projected changes (%) in pAWSSI (upper panel), pAWSSI snow (middle panel) and pAWSSI temperature (lower panel) between 2071-2100 and 1971-2000 under the RCP4.5 scenario.

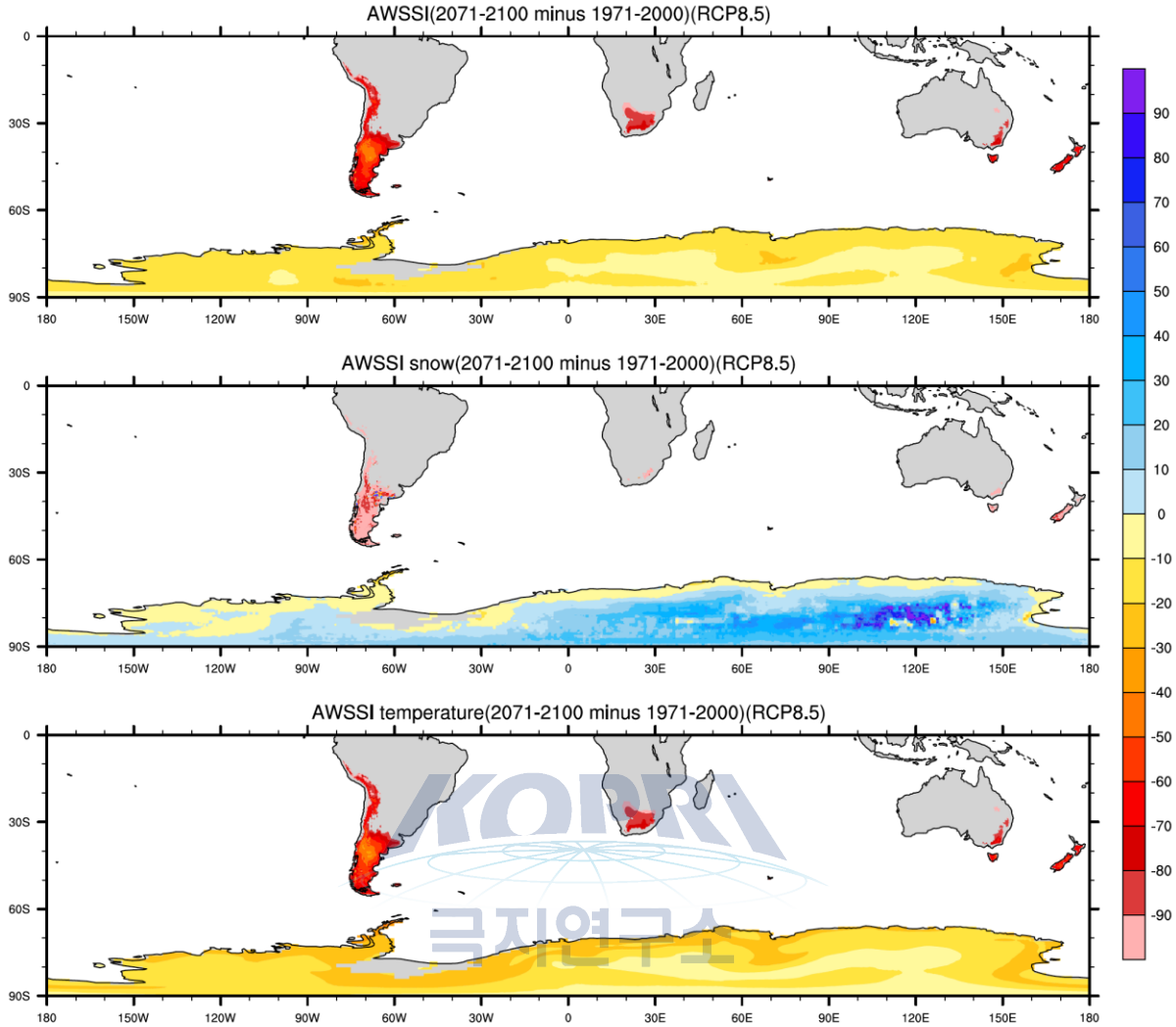

Figure 18: Same as Figure 17 but for the RCP8.5 scenario.

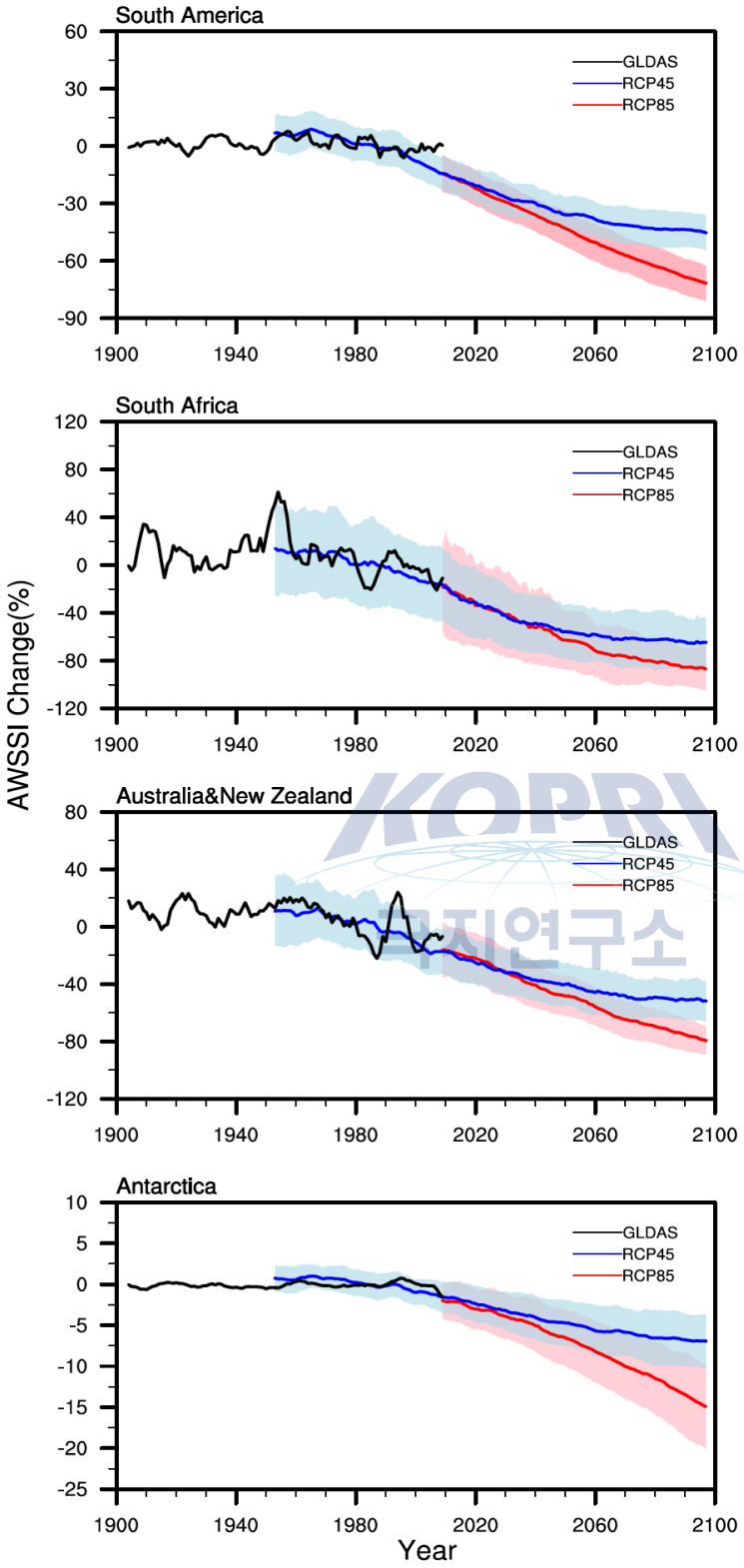

Figure 19. Temporal variations of the regional averaged pAWSSI in the Southern Hemisphere. The black lines are based on GLDAS during 1901-2012. The blues and red lines are the ensemble mean of 21 CMIP5 models during 1951-2100 under RCP4.5 and 8.5 scenarios respectively. The light blue and light red shadings are the 1.0 standardized deviations of the ensemble mean.

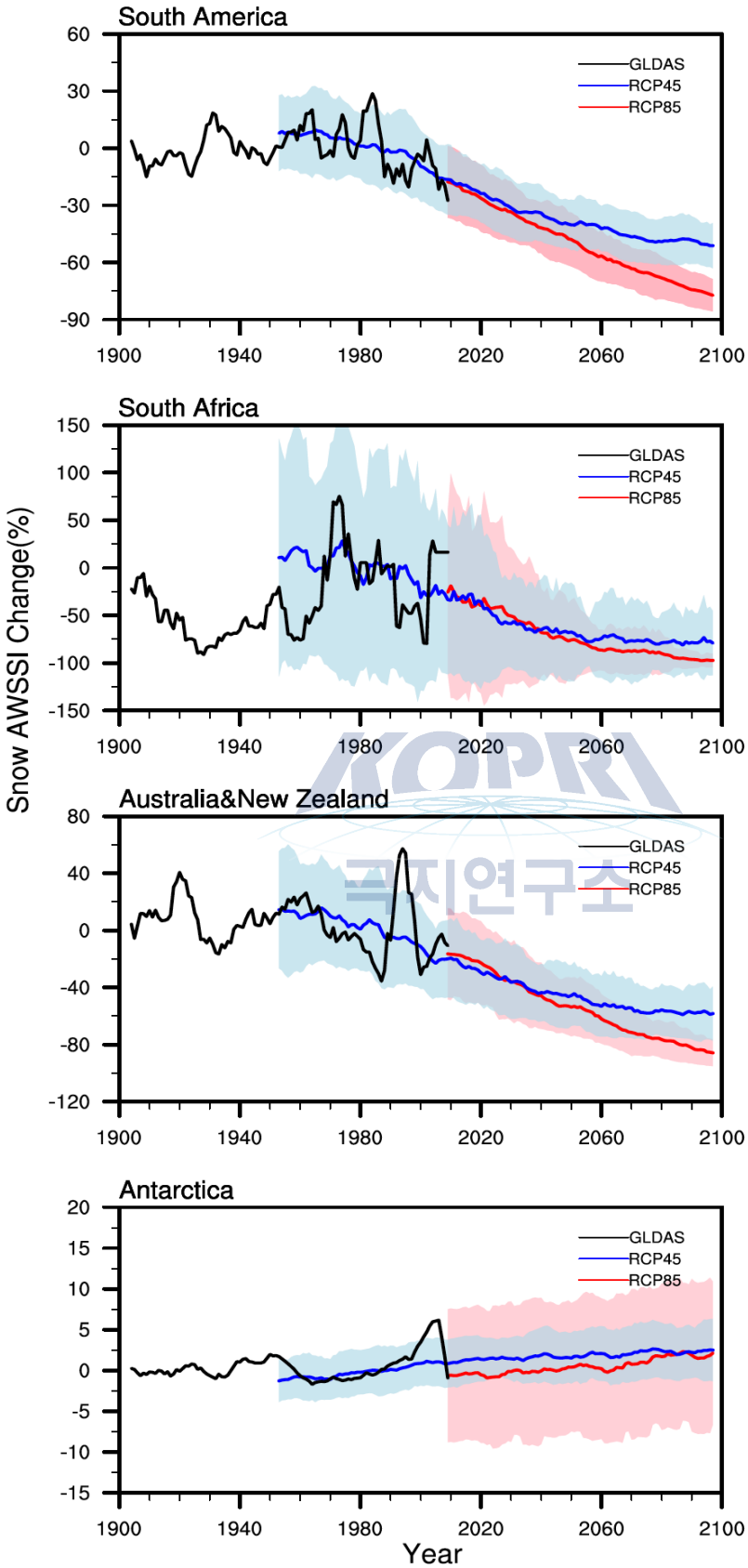

Figure 20. Same as Figure 19 but for pAWSSI_snow.

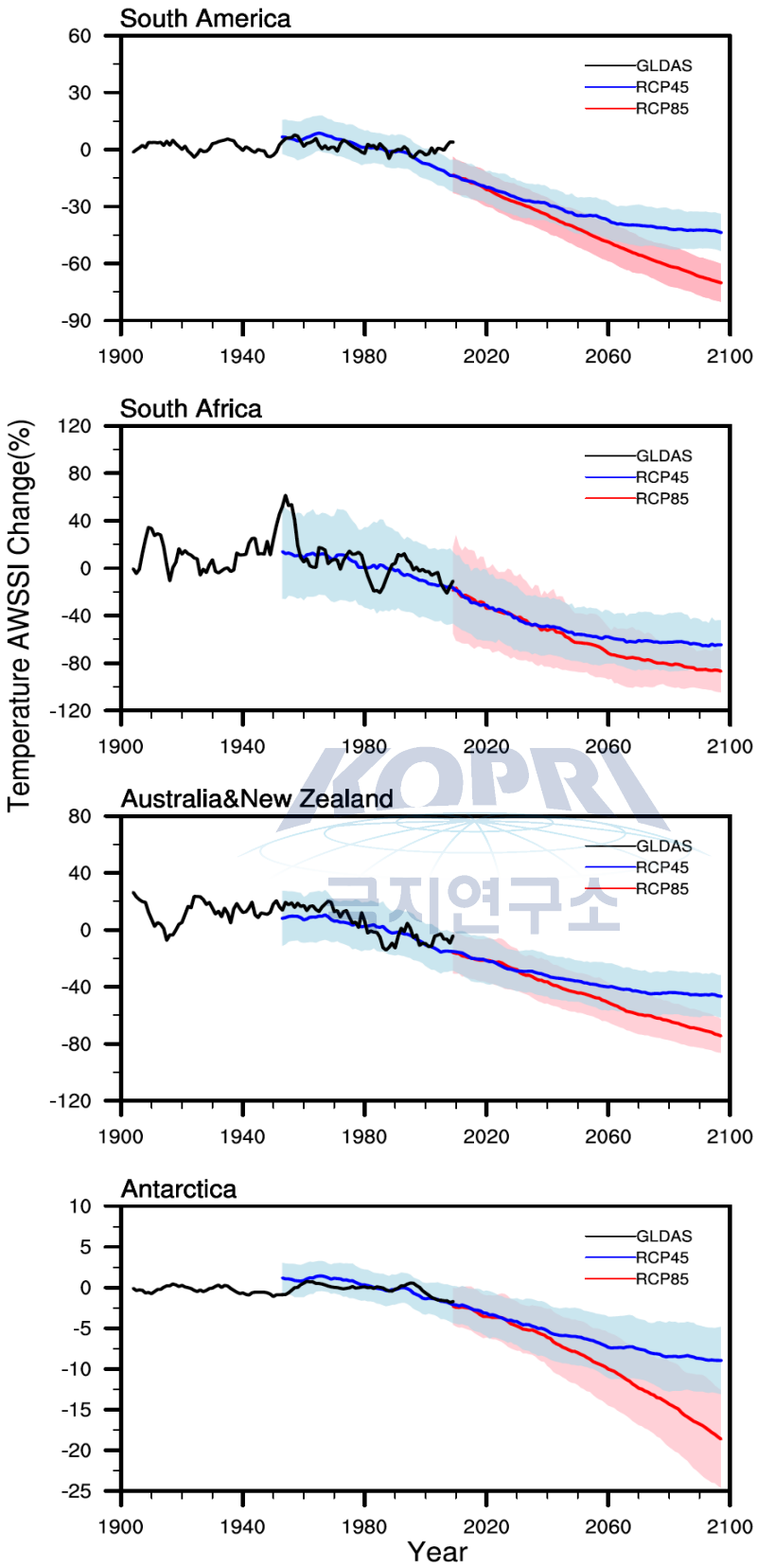

Figure 21. Same as Figure 19, but for pAWSSI_temperature.

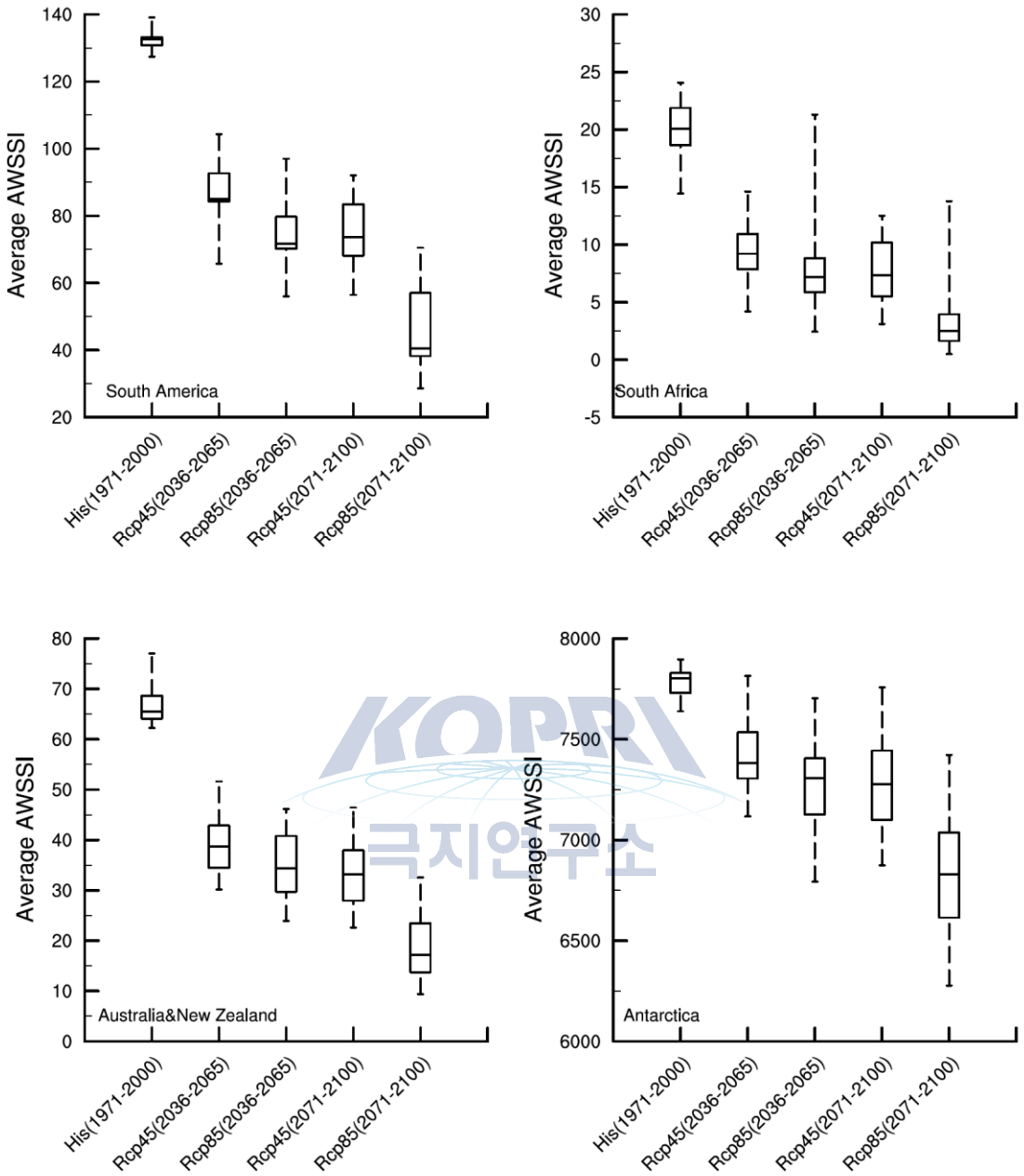

Figure 22. Projected changes in pAWSSI averaged over different continents in the Southern Hemisphere during the middle and the end of this century. The results are plotted with box-and-whisker diagrams representing the areal weighted mean computed from the 21 CMIP5 models. The central line within each box represents the median values of the model simulations. The top and bottom of each box show the 75th and 25th percentiles, and the top and bottom of each whisker display the 95% and 5th percentiles, respectively.

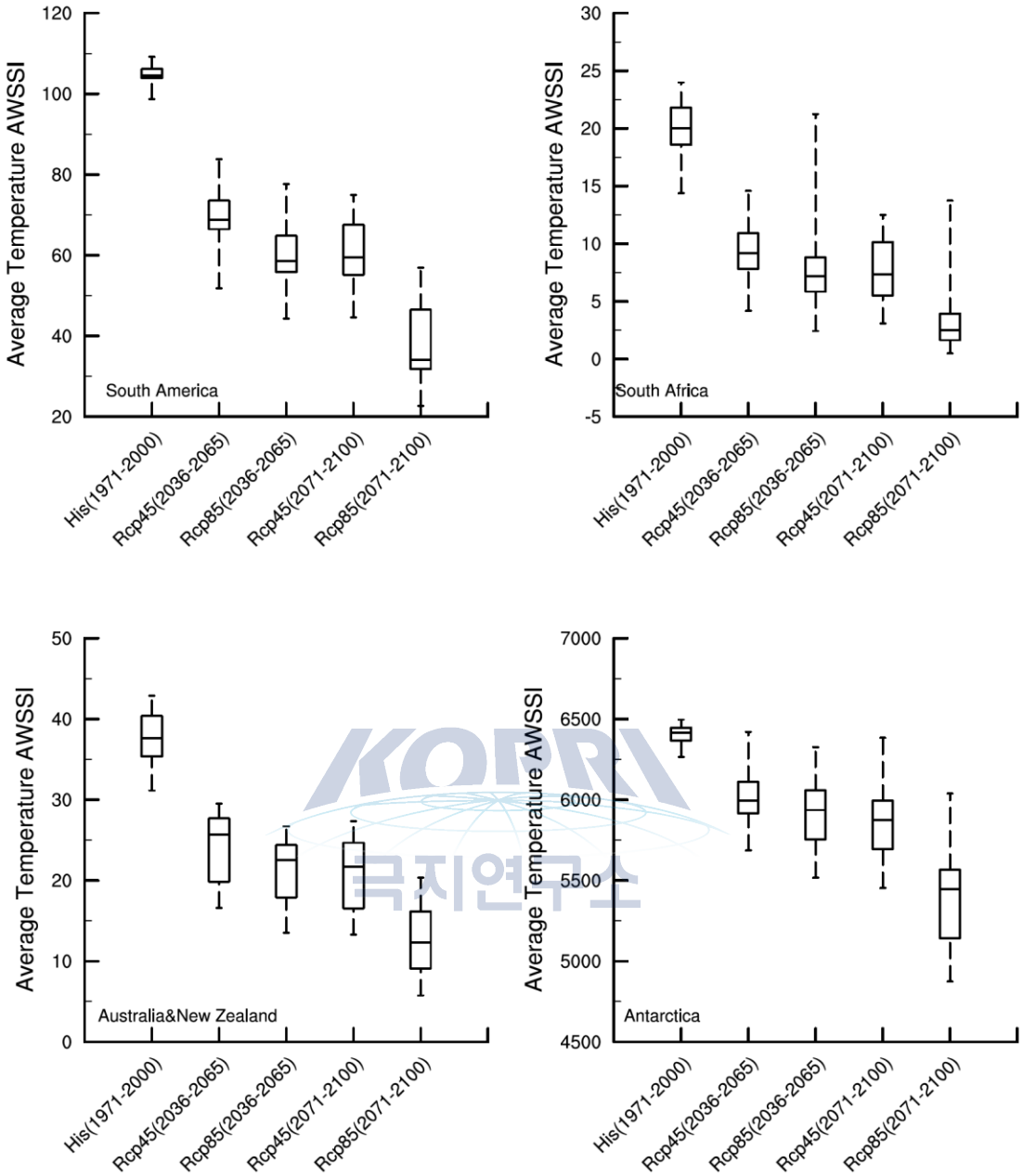

Figure 23. Same Figure 22, but for pAWSSI_temperature.

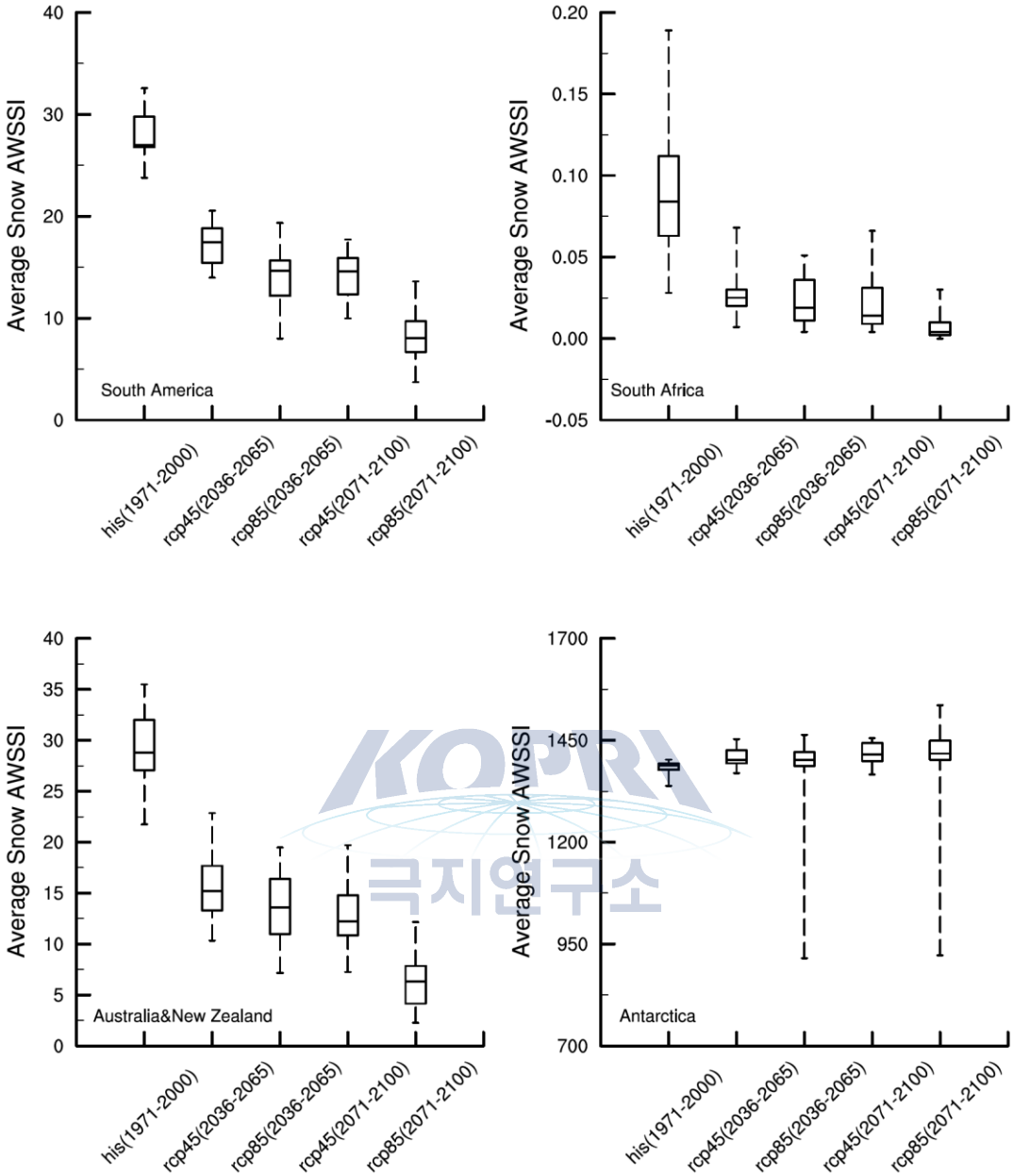

Figure 24. Same Figure 22 but based on pAWSSI_snow.

주 의

1. 이 보고서는 극지연구소 위탁과제 연구결과보고서 입니다.
2. 이 보고서 내용을 발표할 때에는 반드시 극지연구소에서 위탁연구과제로 수행한 연구결과임을 밝혀야 합니다.
3. 국가과학기술 기밀유지에 필요한 내용은 대외적으로 발표 또는 공개하여서는 안됩니다.